Belgian Association for Geomorphologists
Field Trip 4 June 2009

Topic 1: Landscape and processes in the SW-European Cover sand Area during the Last Termination

Topic 2: Late Pleistocene and Holocene surface-rupturing at the Southern border of the Roer Valley Graben

Organizer

Etienne Paulissen
Physical and Regional Geography Research Group
Katholieke Universiteit Leuven

Co-leaders

Kris Vanneste and Koen Verbeeck
Royal Observatory of Belgium

Marijn Van Gils* and Jan Bastiaens
Flemish Heritage Institute
**** Prehistoric research Unit, K.U.Leuven***

Peter Van den haute, Cilia Derese and Dimitri Van den Berghe
Laboratory of Mineralogy and Petrology (Luminescence Research Group
University of Gent

Bas Van Der Veken
Regionaal landschap Kleine en Grote Nete vzw
Landschap De Liereman

Technical Assistance

Bjorn Dieu

Digital version:
http://ees.kuleuven.be/geography/download/bag_excursion_20090604/
http://seismologie.oma.be/dir1600/pdf/BAG2009_FieldTripGuide.pdf

1. Stop 1 – Arendonk - Korhaan

Topics: - Landscape changes during the Last Termination
- The Landscape "De Liereman"

By E. Paulissen, M. Van Gils, J. Bastiaens, B. Van Der Veken, D. Van den Berghe and P. Van den Haute

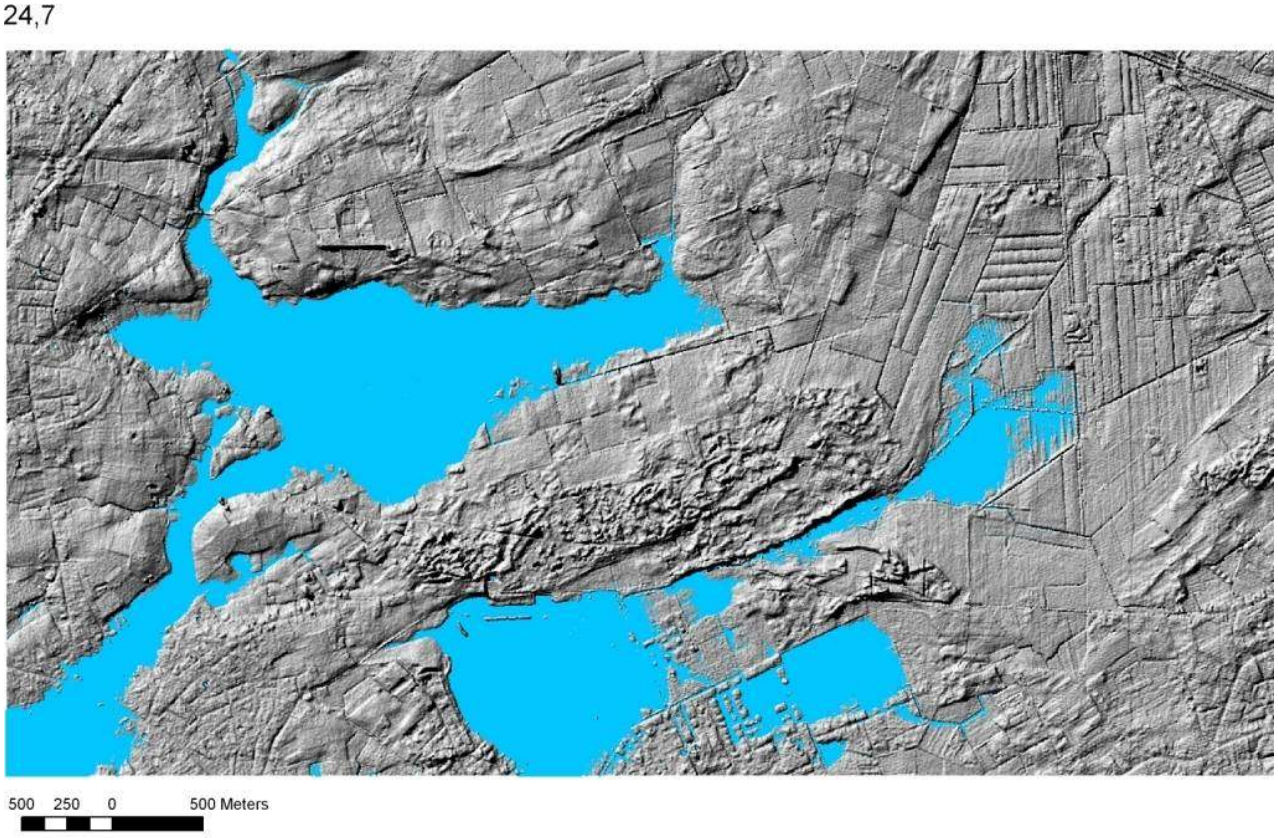

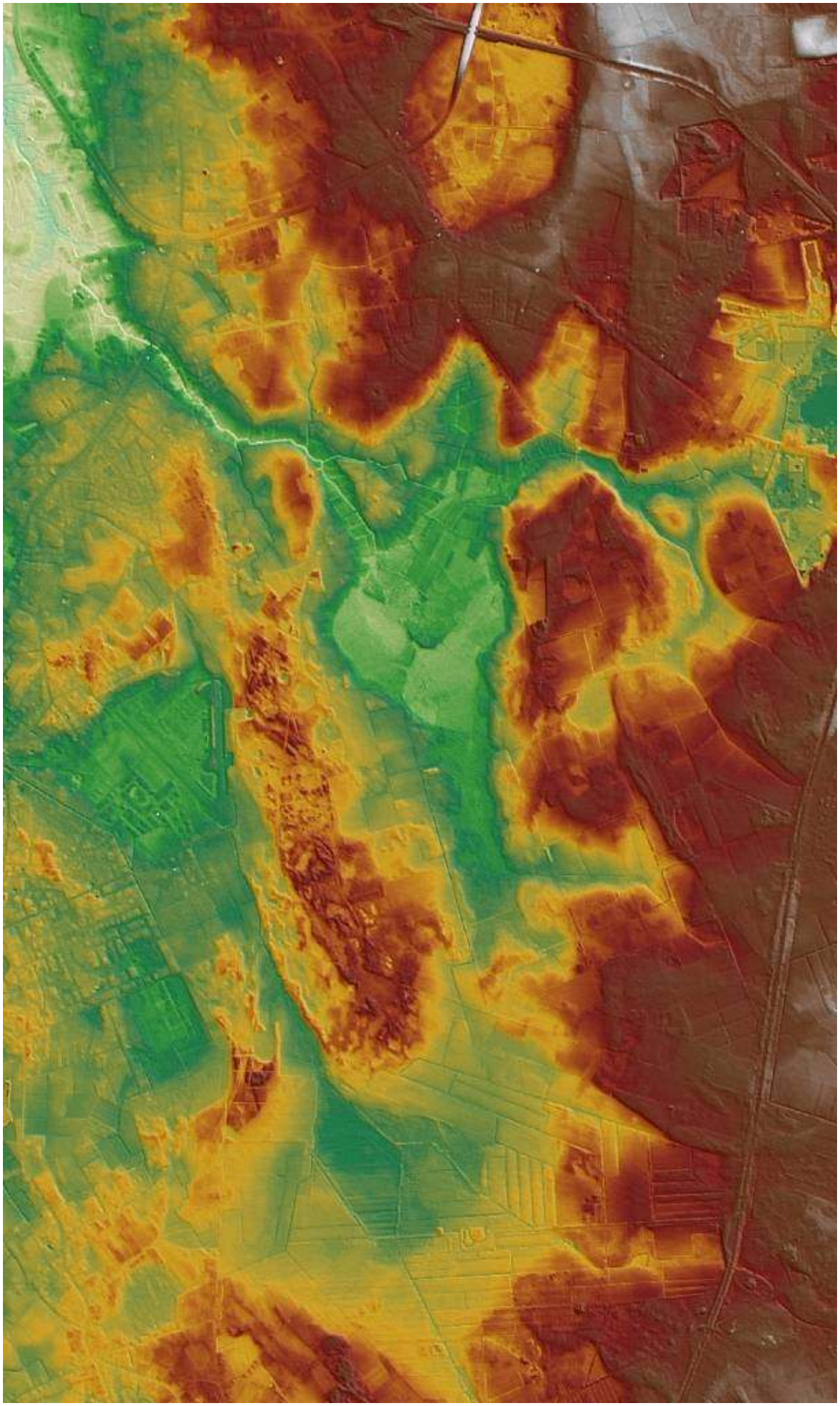

Fig. 1: DEM of the Landscape “De Liereman” and surroundings.

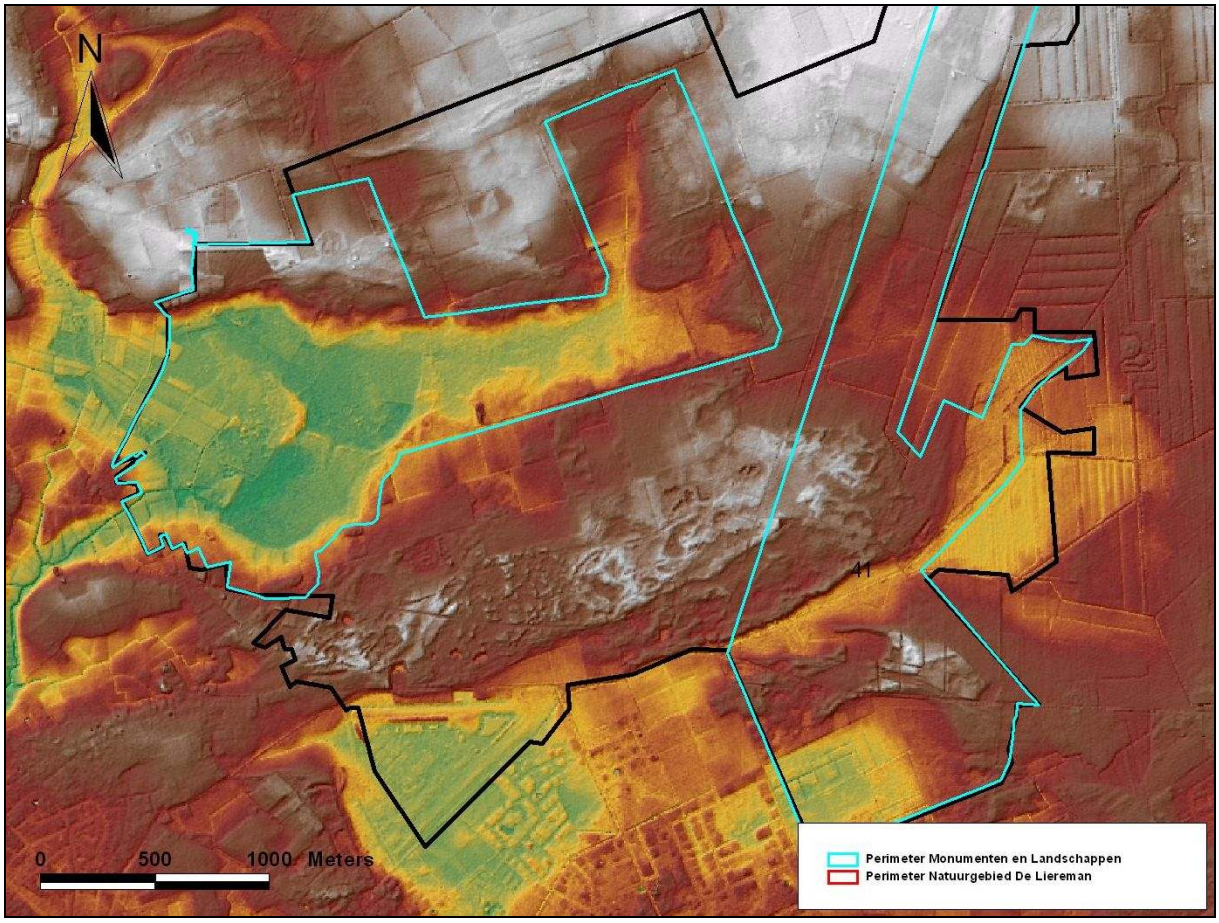

Fig. 2: “Landschap De Liereman” - Limits of the protected landscape (black line) and of the natural area (white line). The digital elevation model is used as background.

Fig. 3: Changes in the Liereman landscape since the 18th century:
The late 18th Century landscape (1775, Ferraris Map, scale ± 1/30.000).

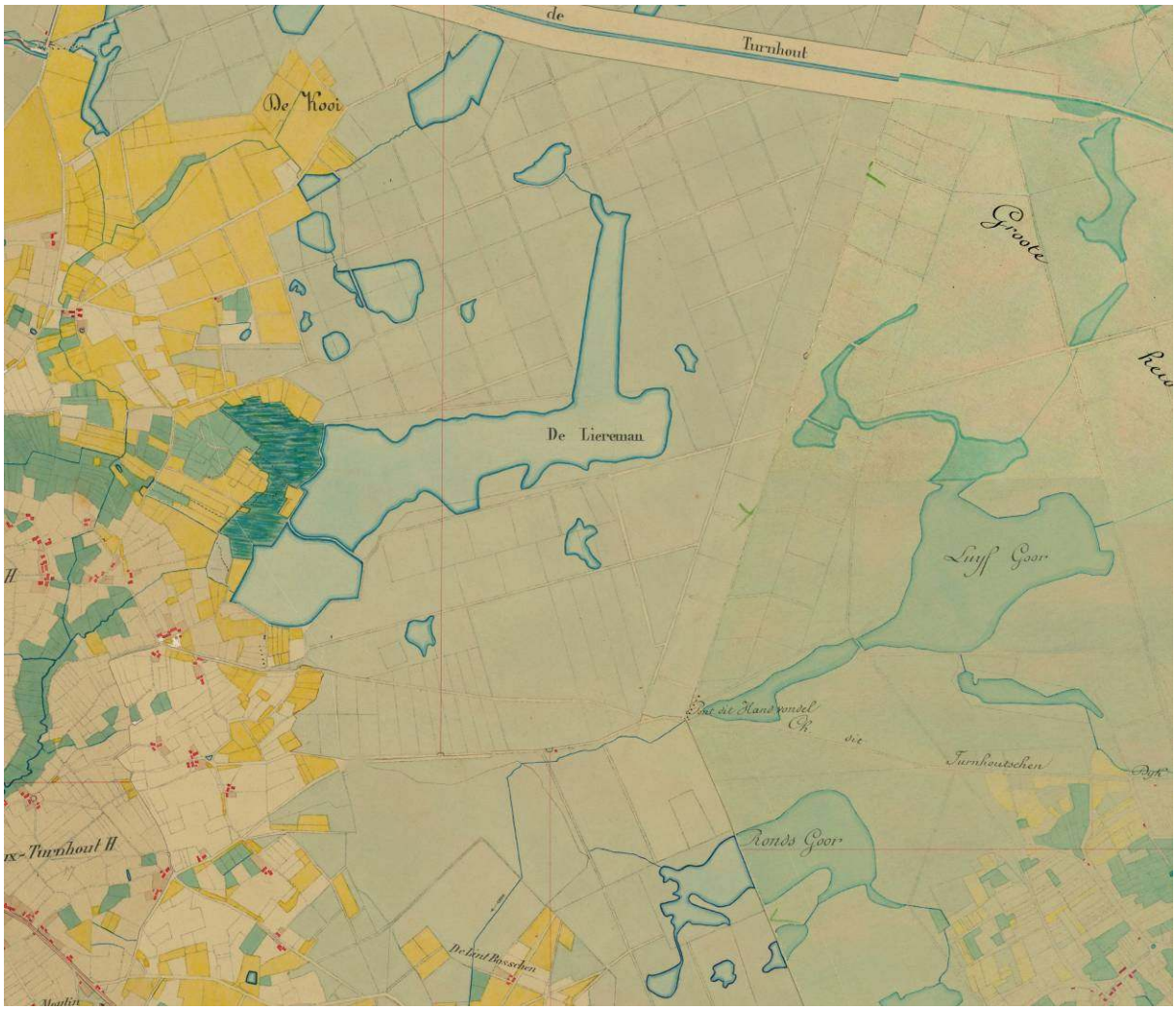

Fig. 4: Changes in the Liereman landscape since the 18th century:
The mid 19th century Landscape (1842, Cadastral Map, scale ± 1/30.000).

Fig. 5: Changes in the Liereman landscape since the 18th century:
The end 19th century landscape (1872, Map Dépôt de la Guerre, scale ± 1/30.000).

Fig. 6: Changes in the Liereman landscape since the 18th century:
The early 20th century landscape (1930, Militair Cartografisch Instituut, scale ± 1/30.000).

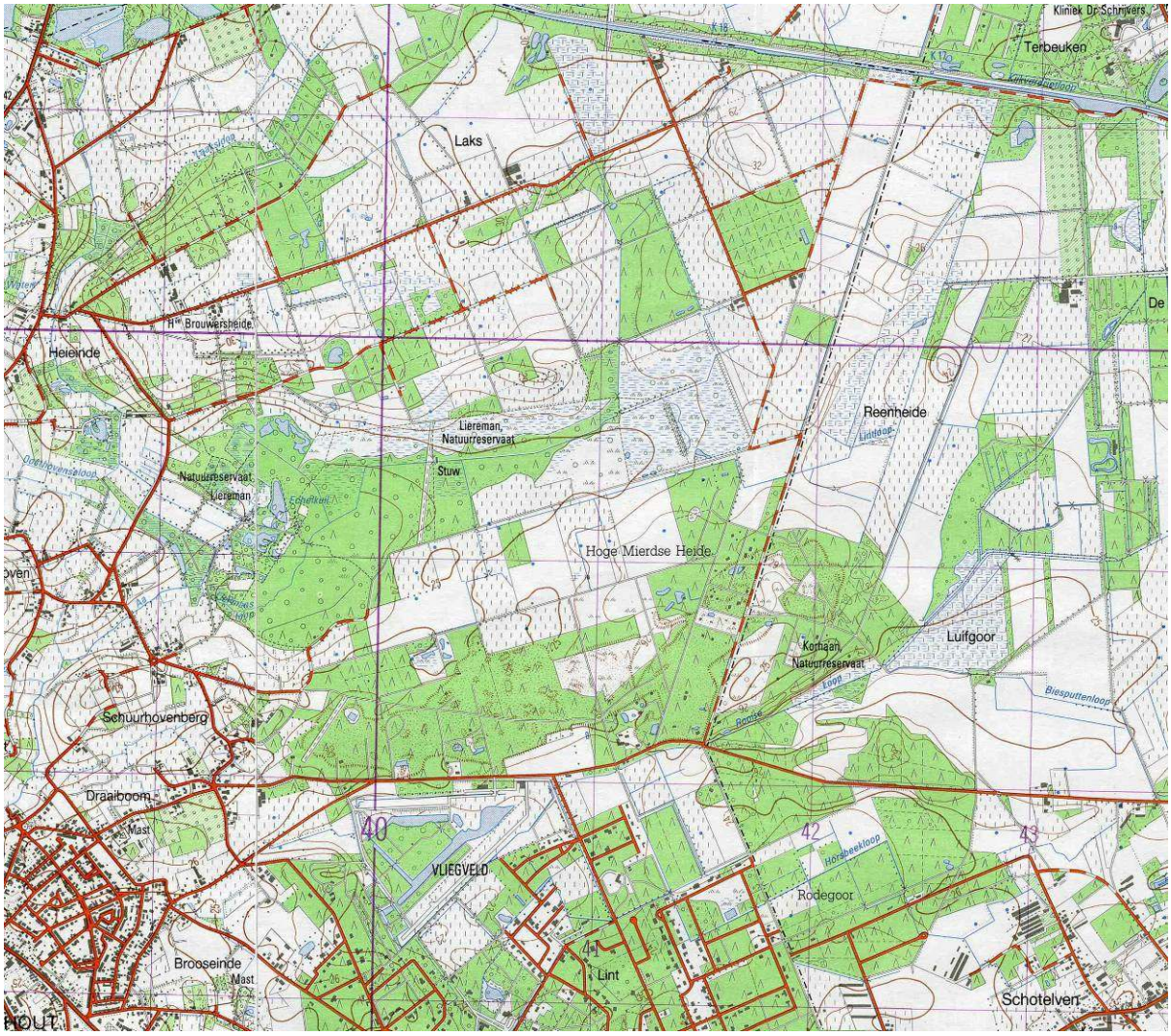

Fig. 7: Changes in the Liereman landscape since the 18th century
The present landscape (1985, Map Nationaal Geografisch Instituut, scale ± 1/30.000).

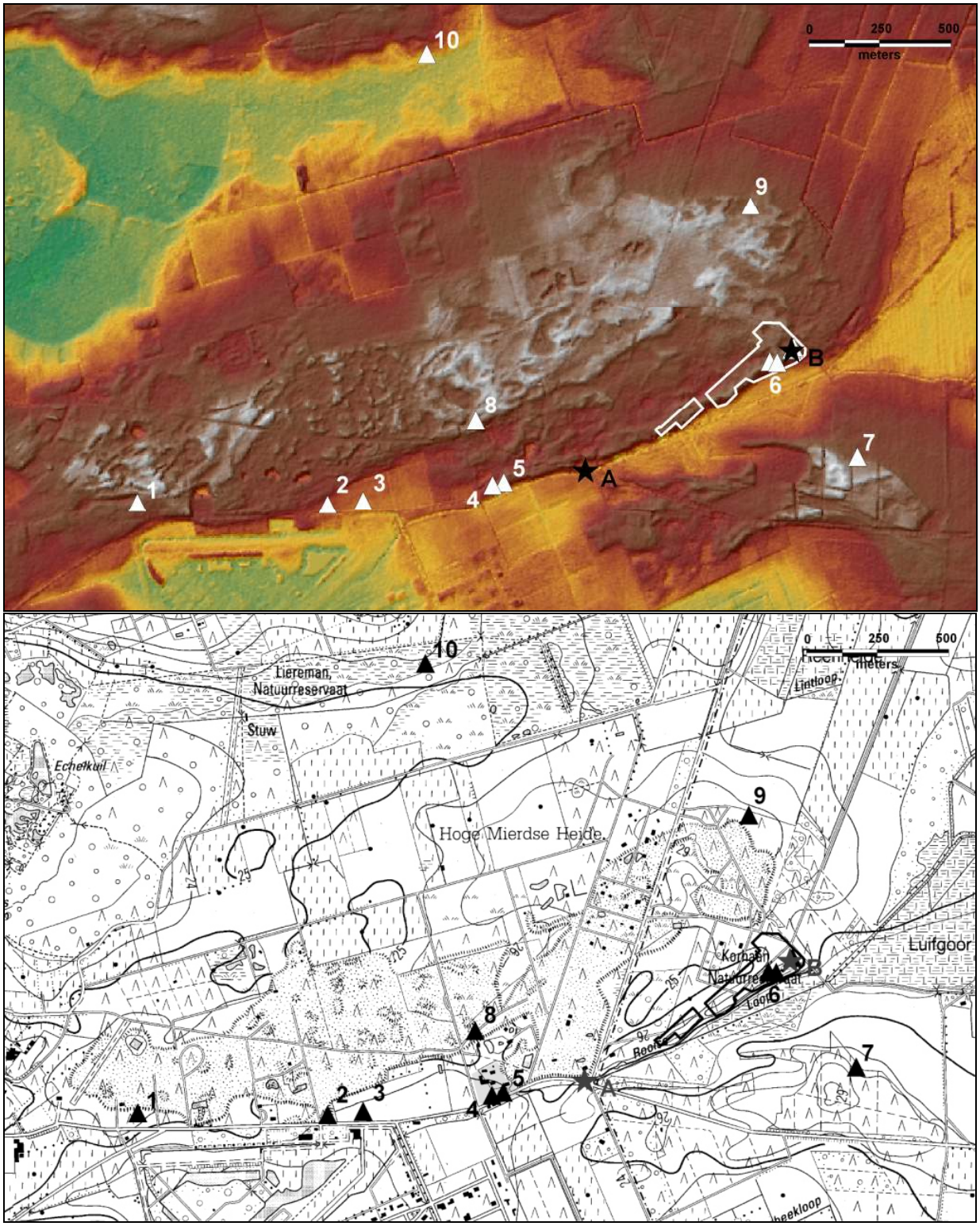

Fig. 8: Location of the prehistoric sites on the DEM and on the topographical map. The line delimits the intensively augered area. (Figure from Meirsman et. al., 2008).

- **A:** Location bus.
- **B:** Location pits A-B-C.
- **1:** Auger finds in podzol.
- **2:** **Oud-Turnhout Bergstraat : auger and testpit finds in Usselo soil.**
- **3:** Oud-Turnhout Bergstraat: surface finds on cropfield.
- **4:** Auger finds in podzol.
- **5:** The first stone-age finds, discovered early in the 20th century.
- **6:** **Arendonk Korhaan: auger and testpit finds in Usselo soil**
- **7:** Auger and surface finds at the south side of the Luifgoor depression.
- **8:** Auger and surface finds in podzol.
- **9:** Auger and surface finds south of Reenheide.
- **10:** Middle Palaeolithic finds north of the Liereman depression.

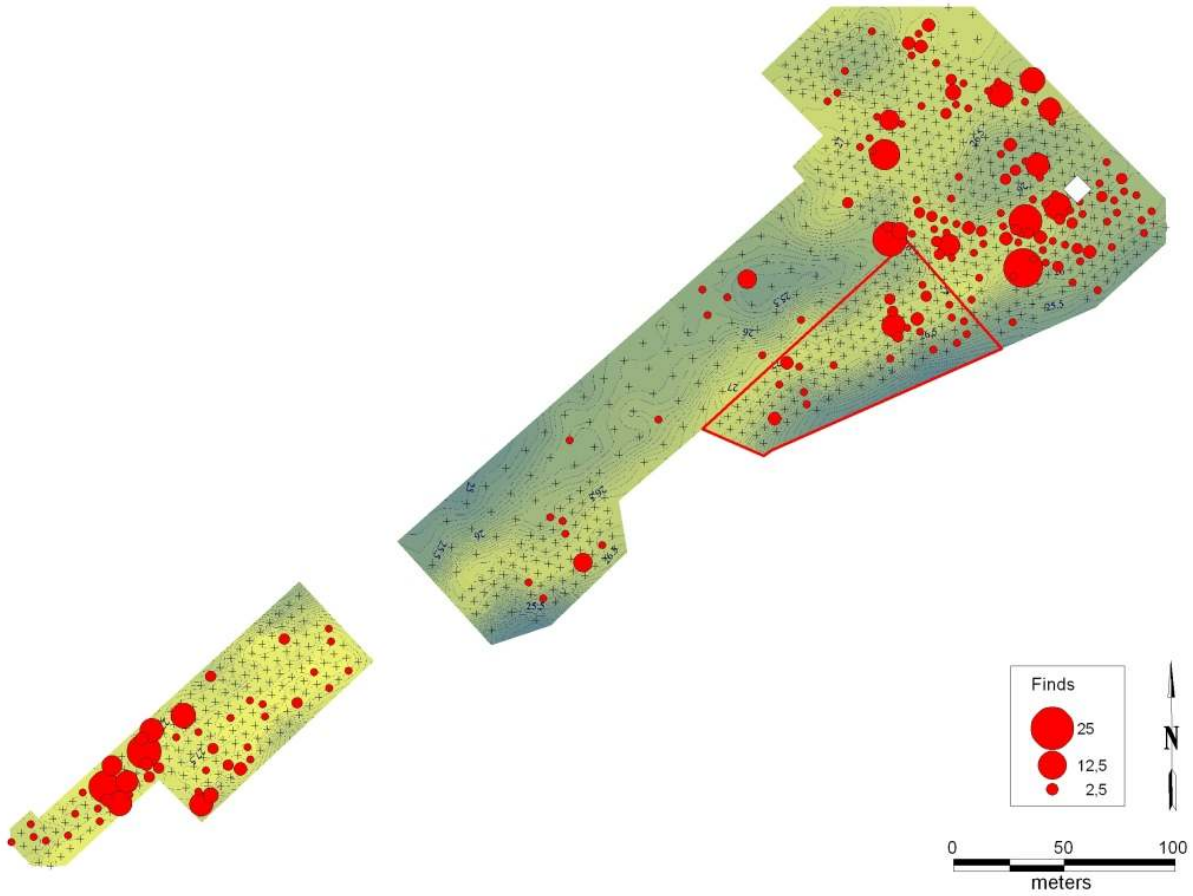

Fig. 9: Topography and distribution of prehistoric finds from the 2003 and 2008 surveys. Augering locations are indicated by small crosses; the dark line delineates the zone surveyed in 2008, and the white square locates pit A (Figure from Van Gils et al., 2009).

+ augering locations

Delineation of the zone surveyed in 2008

pit A

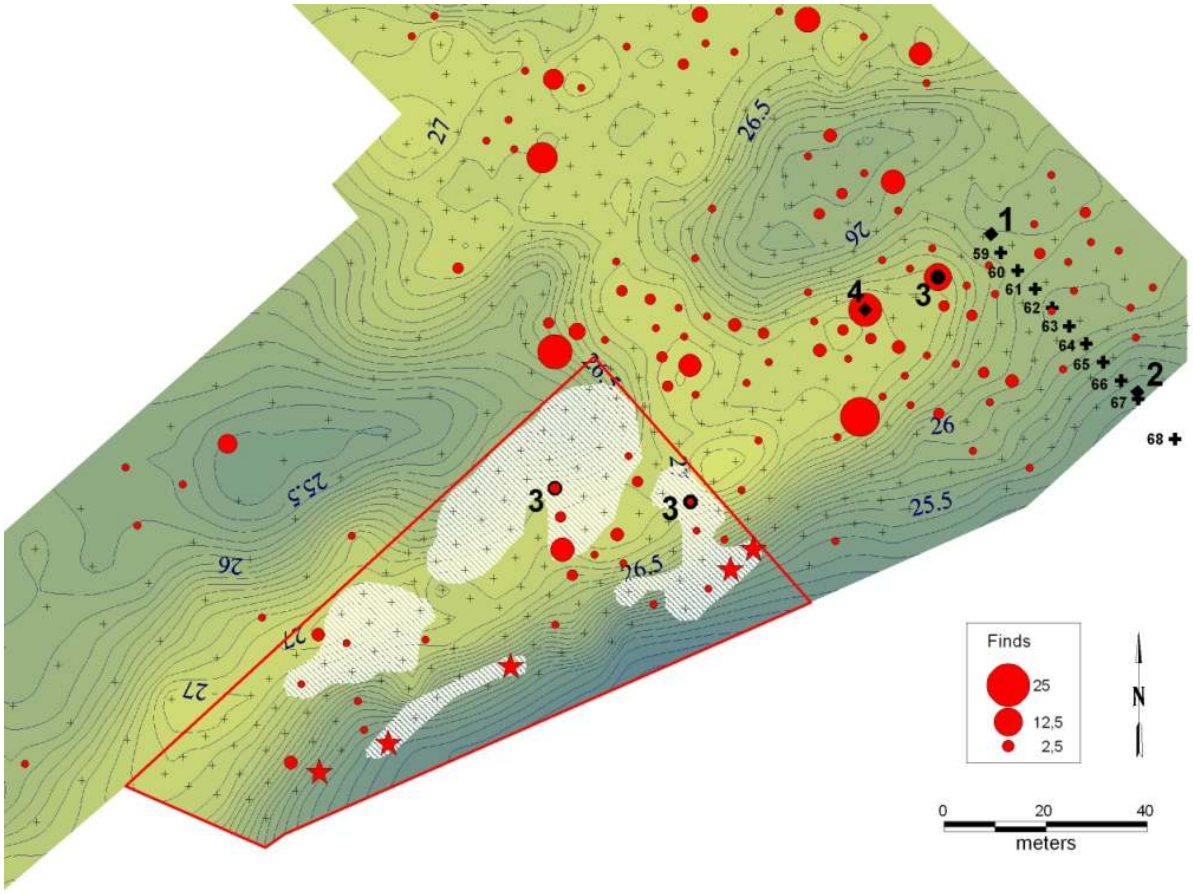

Fig. 10: Distribution of prehistoric finds: in the Korhaan zone.
The dark line delineates the zone surveyed in 2008. (Unpublished Map)

+	augering locations
✚	transect augering locations
	Delineation of the zone surveyed in 2008
1	Pit A
2	Pit B
3	*Auger* locations which yielded finds in Usselo soil
4	Pit C
	presence of clayey sands
	presence of Usselo soil

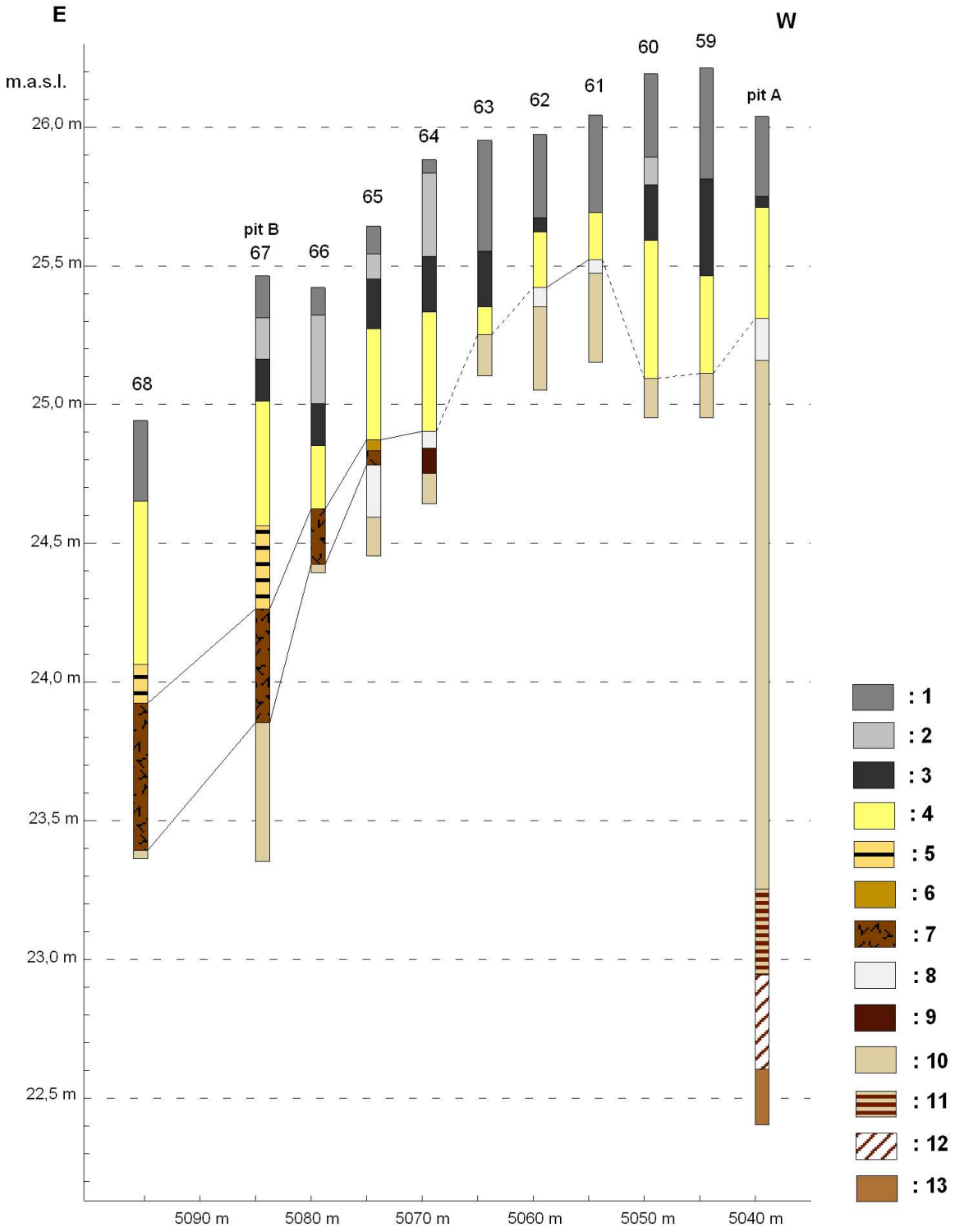

Fig. 11: Korhaan: Core transect and location of pits A and B. The lines between the bore holes suggest the topography on top of the Usselo Soil and the base of the peat unit (unpublished data).

1. Disturbed top soil
2. Podzol soil: E-horizon-
3. Podzol soil: B-horizonl
4. Podzol soil: C-horizon (yellowish sands)
5. Sands with organic layers
6. Clayey sands
7. Peat
8. Usselo soil
9. Dark brown sands
10. Yellowish grey sands
11. Sands with macroscopic plant remains
12. Sands with organic layers
13. Dark brown humic sands

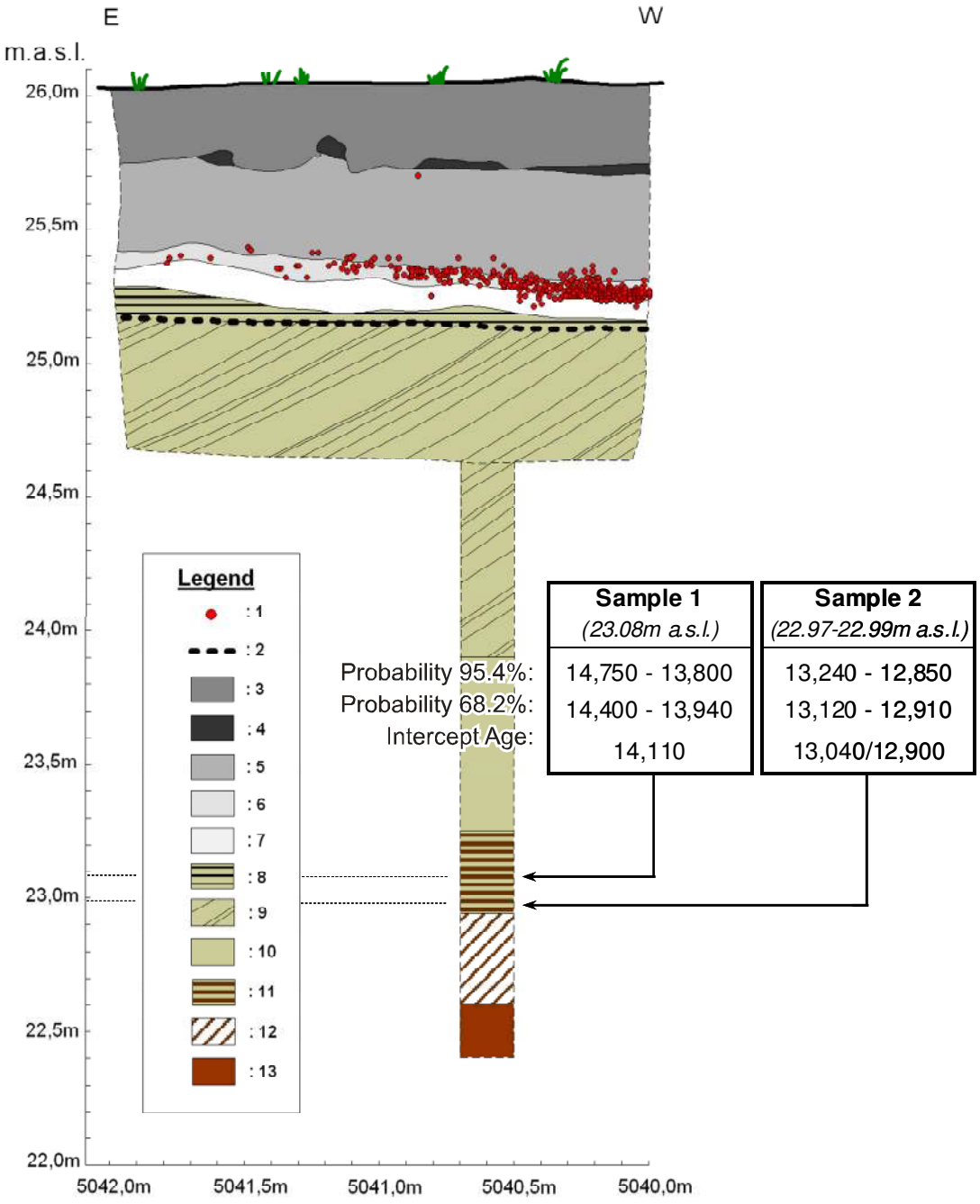

Southern profile of pit A, including augering data:

1. Lithic artefacts
2. Erosion level with gritty layer
3. Disturbed podzol
4. B-horizon podzol
5. Yellowish sands (C-horizon podzol)
6. Silty sands (Usselo soil?)
7. Bleached horizon (Usselo soil)
8. Horizontally layered sands
9. Obliquely layered sands
10. Sands with no visible layering
11. Layer with macroscopic plant remains
12. Sands with organic layers
13. Reddish Brown humic sands

Fig. 12: Korhaan - PIT A – southern wall with coring data and AMS-ages (unpublished)

Fig. 13: Korhaan – Pit A - southern wall. The inclinations of the sand deposits underneath the Usselo soil are clearly visible. They are built up by North-Western winds.

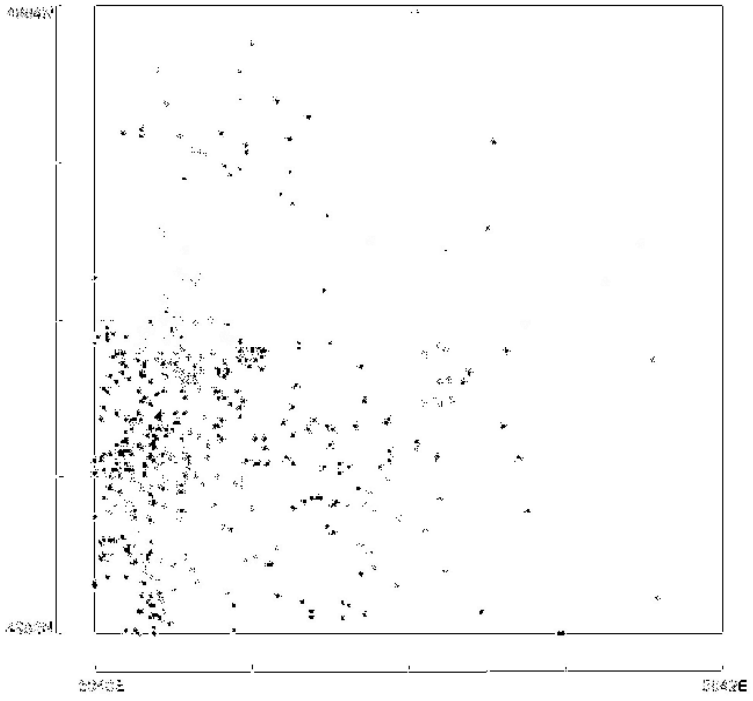

Fig. 14: Korhaan – Pit A – Horizontal plan showing the distribution of flint artefacts in the silty layer just above the whitish layer, typical for the Usselo soil. (Figure from Meirsman et. al., 2008).

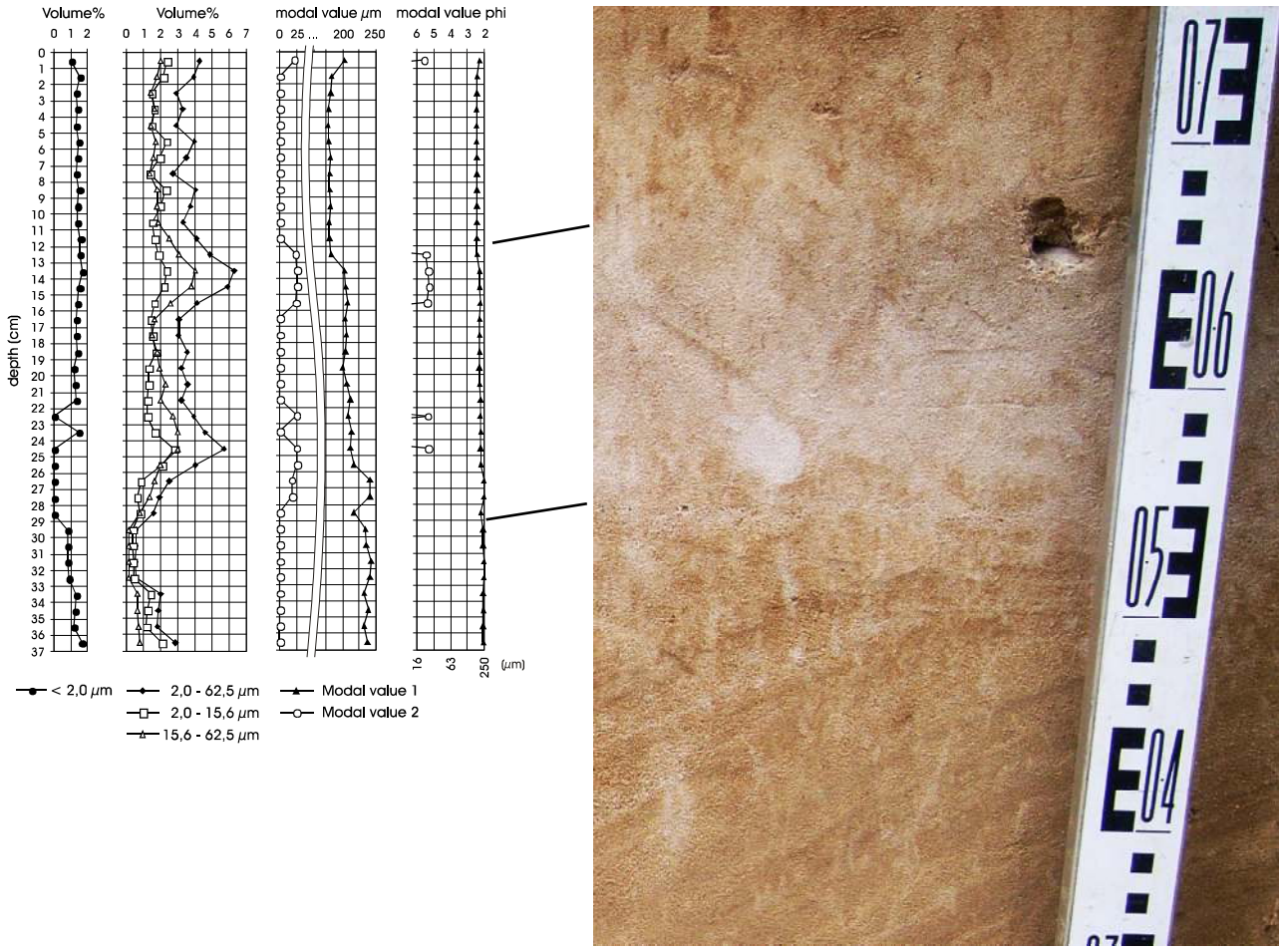

Fig. 15: Korhaan – Pit A – Usselo Soil: grain size

1) AMS ages

Each AMS-age on one piece of charcoal
Ages in cal yr BP (INTCAL04)

Charcoal from Upper bleached layer

	Charcoal 1	Charcoal 2
Probability 95.4%:	12,940 - 12,800	12,700 - 12,100
Probability 68.2%:	12,895 - 12,830	12,640 - 12,370
Intercept Age:	12,860	12,398

Charcoal from Lower bleached layer

	Charcoal 3	Charcoal 4
Probability 95.4%:	13,320 - 12,910	13,060 - 12,860
Probability 68.2%:	13,320 - 12,910	12,975 - 12,880
Intercept Age:	13,130	12,920

2) OSL ages – beneath bottom Usselo soil

50-55cm: 14.8 ± 1.2 ka

80-85cm: 14.5 ± 1.1 ka

Fig. 16: Northern profile of the pit C. AMS and OSL ages (unpublished data). AMS ages of individual charcoal pieces from the two whitish layers diverging from one whitish layer point to the Allerød period.

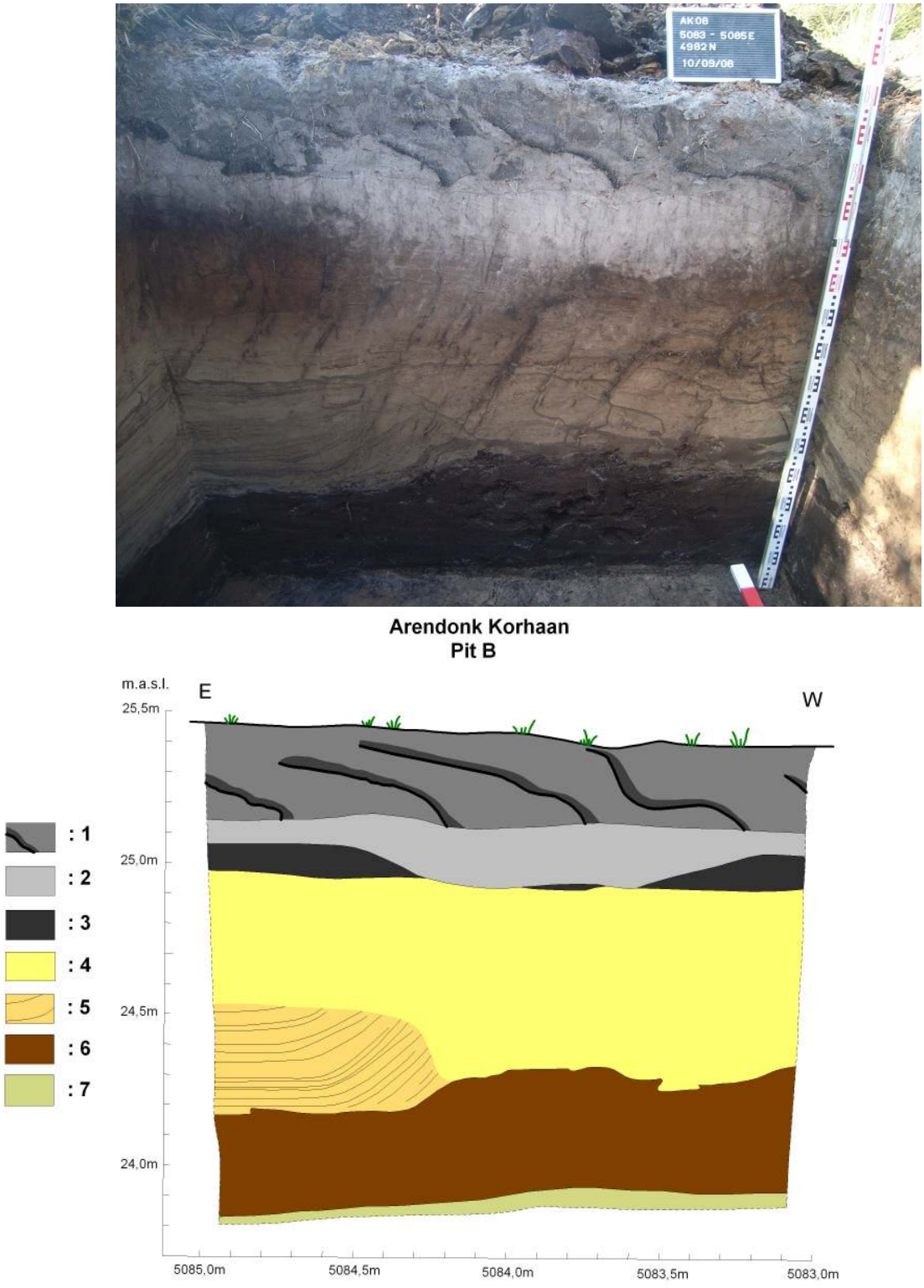

Fig. 17: Korhaan – Pit B - Southern wall with AMS ages (unpublished data).

1. Disturbed top soil with plough marks
2. Podzol - E-horizon
3. Podzol - B-horizon
4. Podzol – C-horizon (Yellowish sands)
5. Stratified sands alternating with organic layers – situated towards the depression
6. Horizontally stratified peat
7. Horizontally stratified sand and organic layers

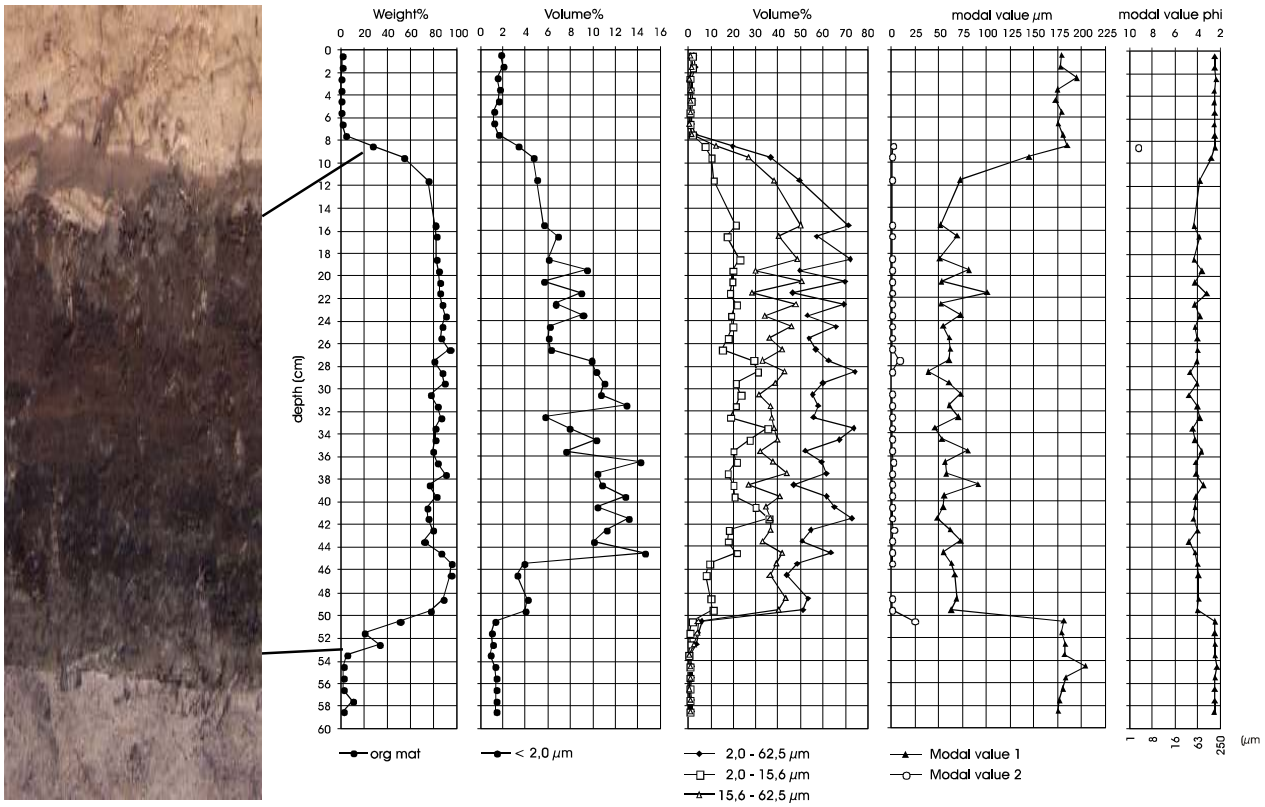

AMS-ages on uncharred seeds
Ages in cal yr BP (INTCAL04)

AMS age top Peat

	Sample 1 at about 10 cm
Probability 95.4%	13,070 - 12,850
Probability 68.2%	12,980 - 12,870
Intercept Age	12,990

AMS ages base Peat

	Sample 1 at 44 cm	**Sample 2** at about 44cm	**Sample 3** at 46 cm
Probability 95.4%	13,980 - 13,700	13,240 - 12,850	14,600 – 13,950
Probability 68.2%	13,890 - 13,750	14,080 - 13,790	14,270 – 14,030
Intercept Age	13,805	13,940	14,145

Fig. 18: Korhaan- PIT B-peat layer: detritic matter content, grain size and AMS dates for its top and bottom (unpublished data)

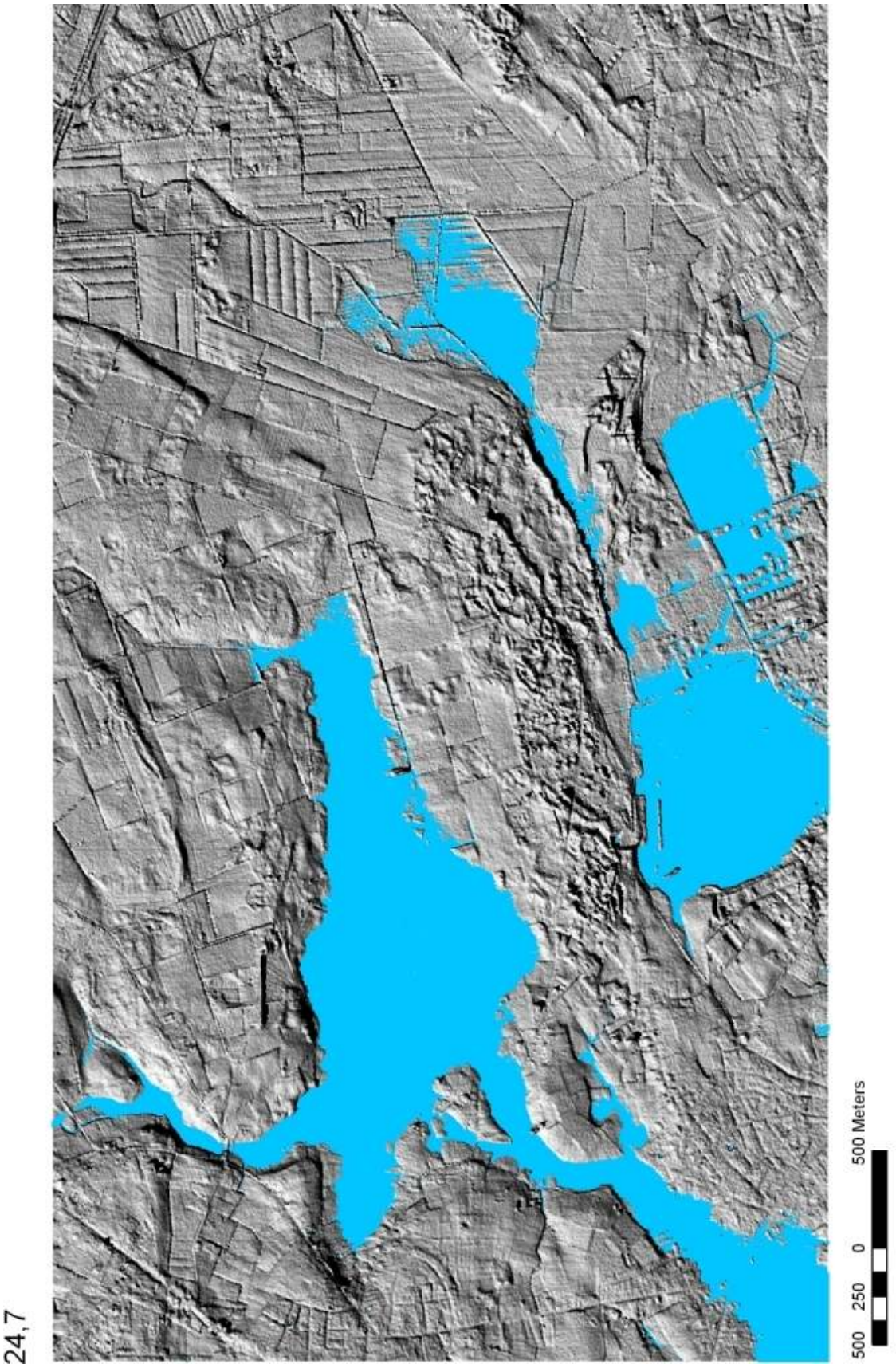

Fig. 19: Simulation of the physical landscape during Allerød time starting from the present relief as mapped on the DEM. The uniform grey surface is thought to represent the minimum extent of the marsh at the borders and an eventual water surface in the middle (?). Its height is at 24.7 m a.s.l. and corresponds with the top of the present peat surface in pit B (see Fig. 17).

References

DE BIE, M. & VAN GILS, M., 2009 in press, Mesolithic settlement and land use in the Campine region (Belgium). In: MCCARTAN S., SCHULTING R., WARREN G. & WOODMAN P. (red.), Mesolithic Horizons. Proceedings of the seventh international conference on the Mesolithic in Europe (Belfast 2005), Oxbow, Oxford.

DE LOË, A., 1905, Station Néolithique et tombelle (?) à Vieux-Turnhout (Province d'Anvers), *Annuaire de la Société Royale d'Archéologie de Bruxelles*, 19, 146-147.

HAEST, R., 1985, Invloed van het Weichsel-Glaciaal op de geologie van de Noorderkempen. Doctoraatsverhandeling K. U. Leuven.

MEIRSMAN, E., VAN GILS, M., VANMONTFORT, B., PAULISSEN, E., BASTIAENS, J. & VAN PEER, P., 2008, Landschap De Liereman herbezocht. De waardering van een gestratifieerd finaalpaleolithisch en mesolithisch sitecomplex in de Noorderkempen (gem. Oud-Turnhout en Arendonk), *Notae Prehistoricae* 28, 33-41.

STROOBANT, L., 1903, Exploration de quelques tumuli de la Campine Anversoise, *Annales de l'Académie Royale d'Archéologie de Belgique*, 54, 394-395.

VAN GILS, M. & DE BIE, M. 2003, Kartering en waardering van een Mesolithisch site-complex te Arendonk 'Korhaan', *Notae Praehistoricae* 23, 67-69.

VAN GILS, M. & DE BIE, M. 2008, Les occupations tardiglaciaires et postglaciaires du nord de la Belgique: modalités d'occupation du territoire. In: FAGNART, J.-P., THEVENIN, A., DUCROCQ, T., SOUFFI, B. & COUDRET, P. (eds): *Le début du Mésolithique en Europe du Nord-Ouest* (Mémoires XLV de la Société préhistorique française), 205-218.

VAN GILS, M., DE BIE, M., PAULISSEN, E. & DEFORCE, K., 2009, Kartering en waardering van een finaalpaleolithisch/mesolithisch sitecomplex te Arendonk Korhaan (prov. Antwerpen). Boorcampagne 2003, *Relicta* 4, 9-21.

2. Stop 2 – Bree - Southern border of the Roer Valley Graben

Topics: Late Pleistocene and Holocene surface-rupturing

By K. Vanneste, K. Verbeek, E. Paulissen and D. Van den Berghe

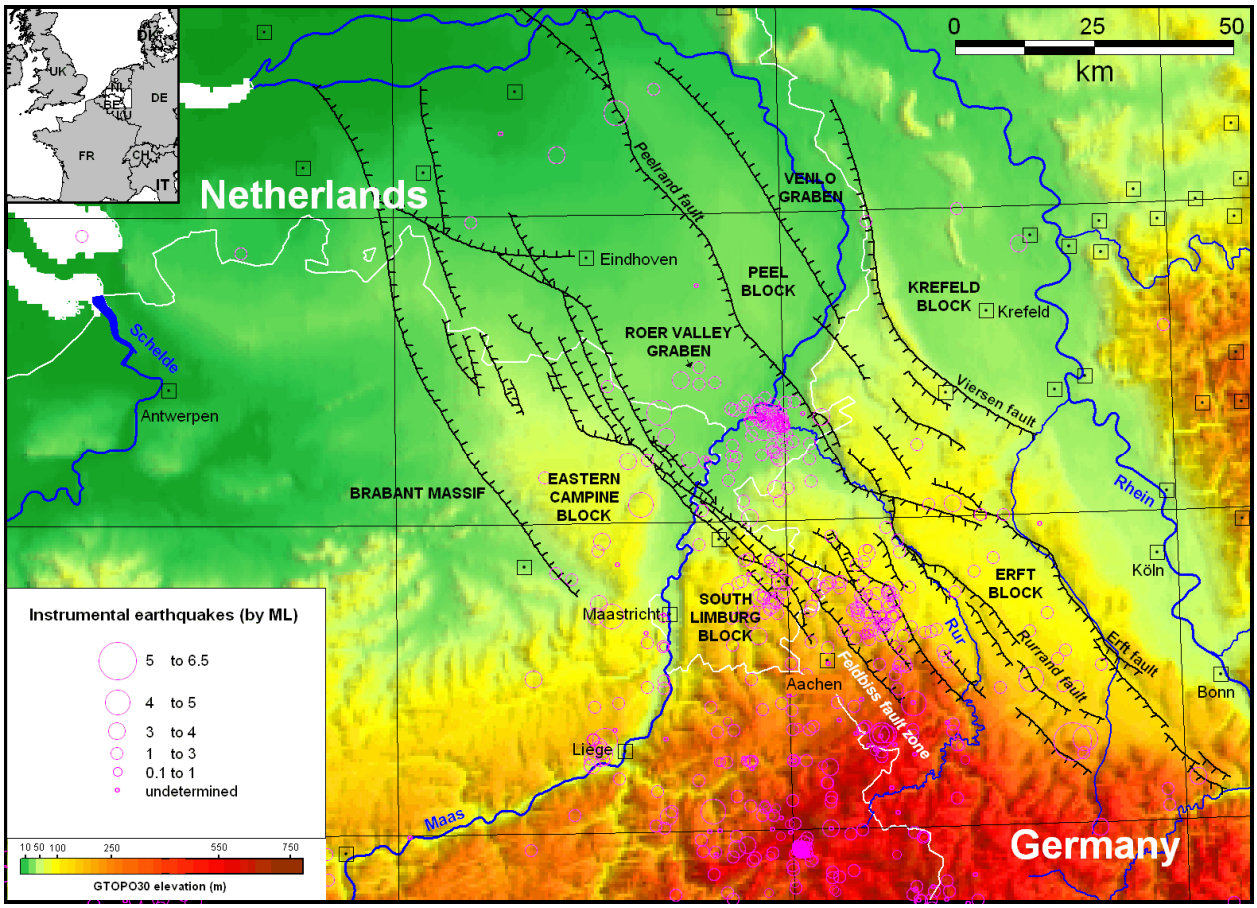

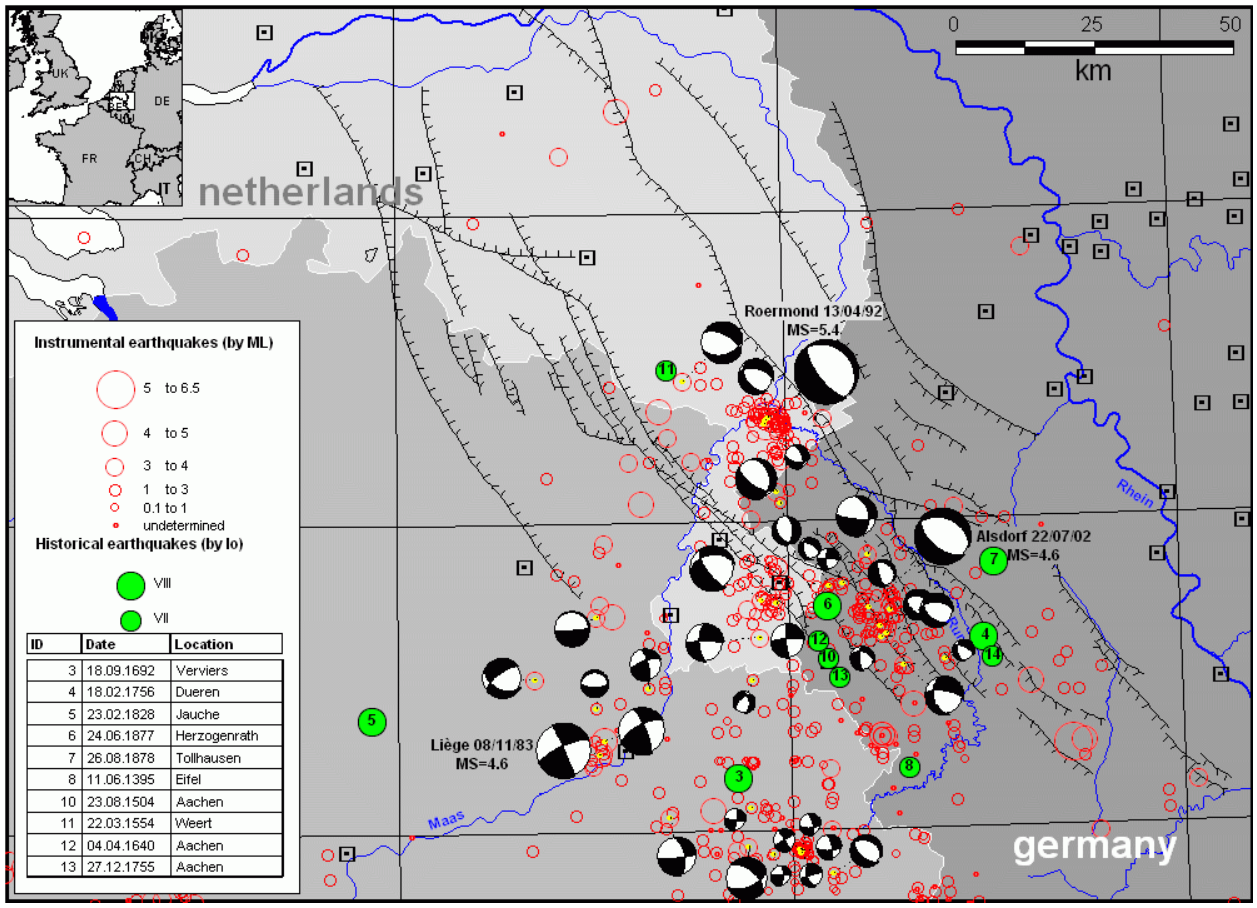

Figs. 20 and 21 – Seismicity and Quaternary faults in the Lower Rhine Graben area

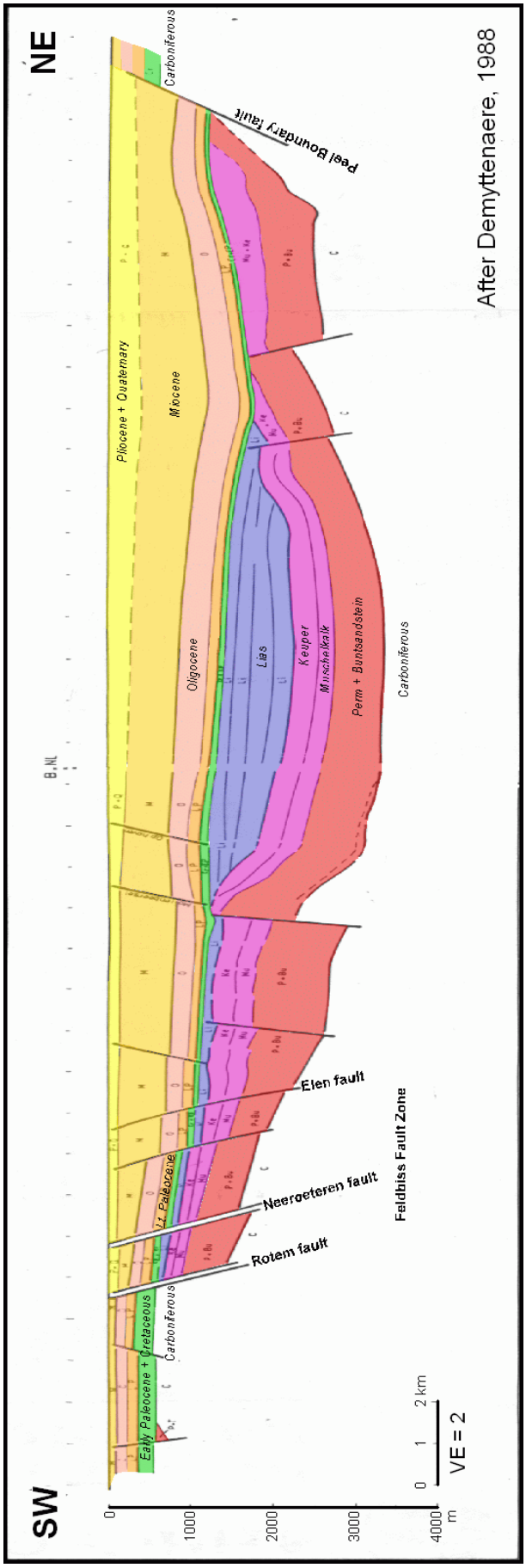

Fig. 22 – Geological cross-section through the Roer Valley Graben (after Demyttenaere, 1988).

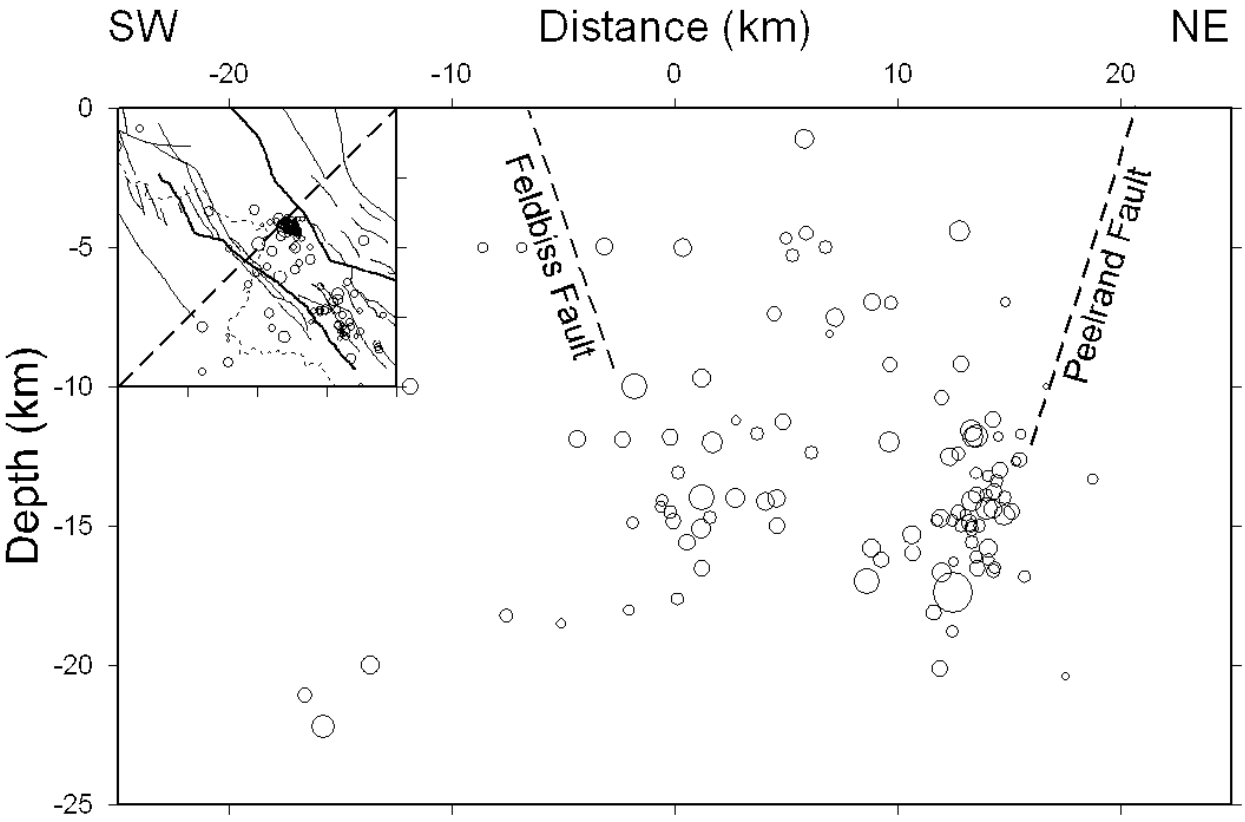

Fig. 23 – Seismicity cross-section of the Roer Valley Graben.

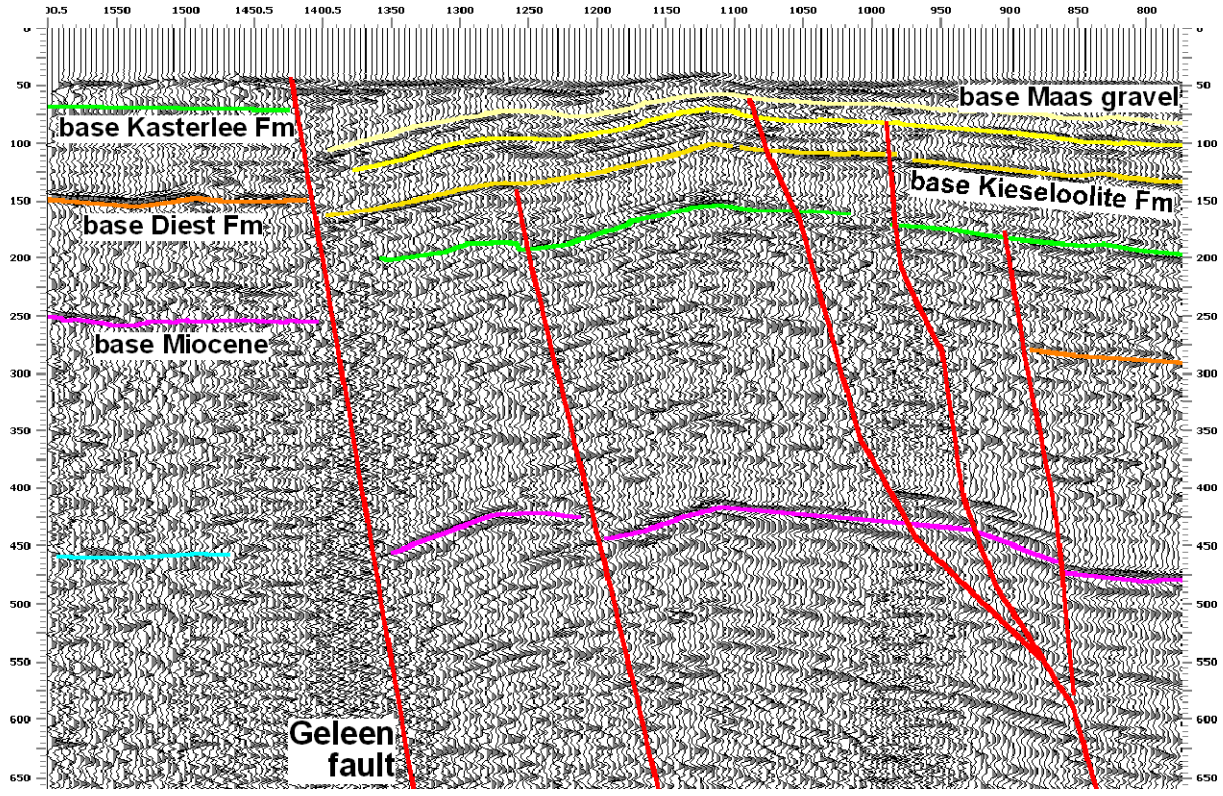

Fig. 24 – Seismic-reflection profile across the Feldbiss fault zone in Belgium (Figure taken from Dusar et al., 2001).

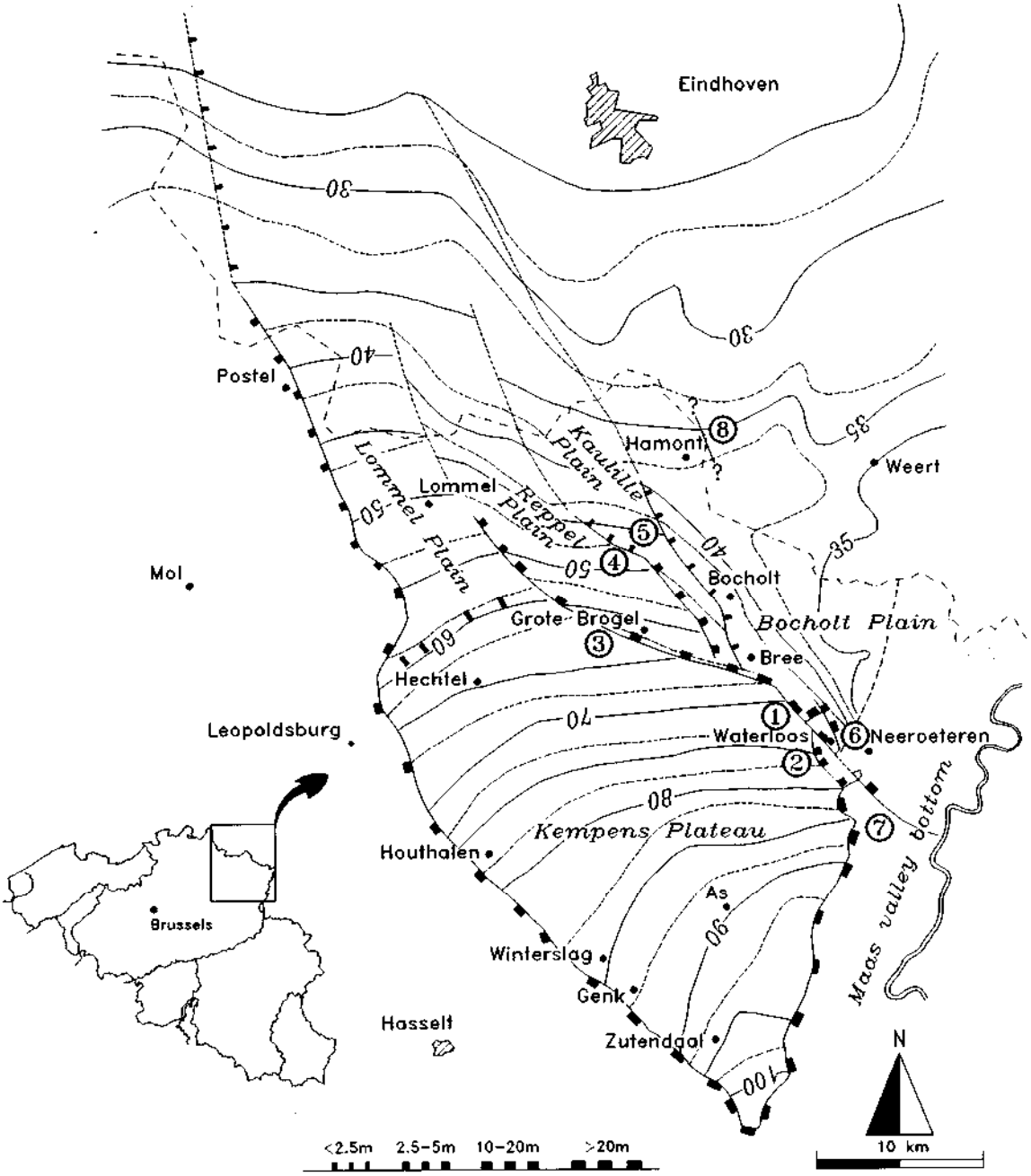

Fig. 25: Faults at the south-western border of the Roer Valley graben, the result of geomorphological mapping, including the height of the morphological scarps. Figure taken from Paulissen (1997).

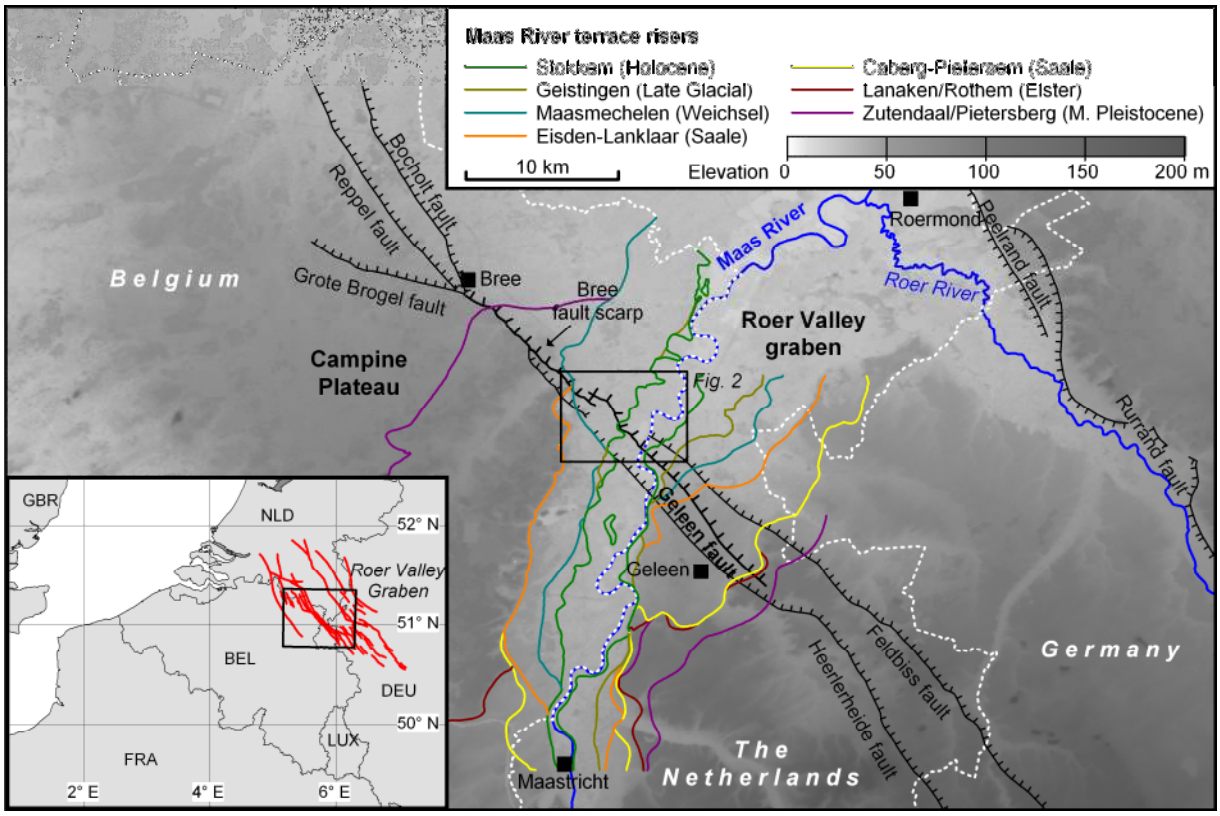

Fig. 26 – Map of the south-western border of the Roer Valley graben showing the main faults and the Maas River terraces (after Felder et al., 1989 in The Netherlands, and Beerten et al., 1998 in Belgium). Box indicates study area shown in Figs. 20 and 21. Figure taken from Vandenberghe et al. (2009).

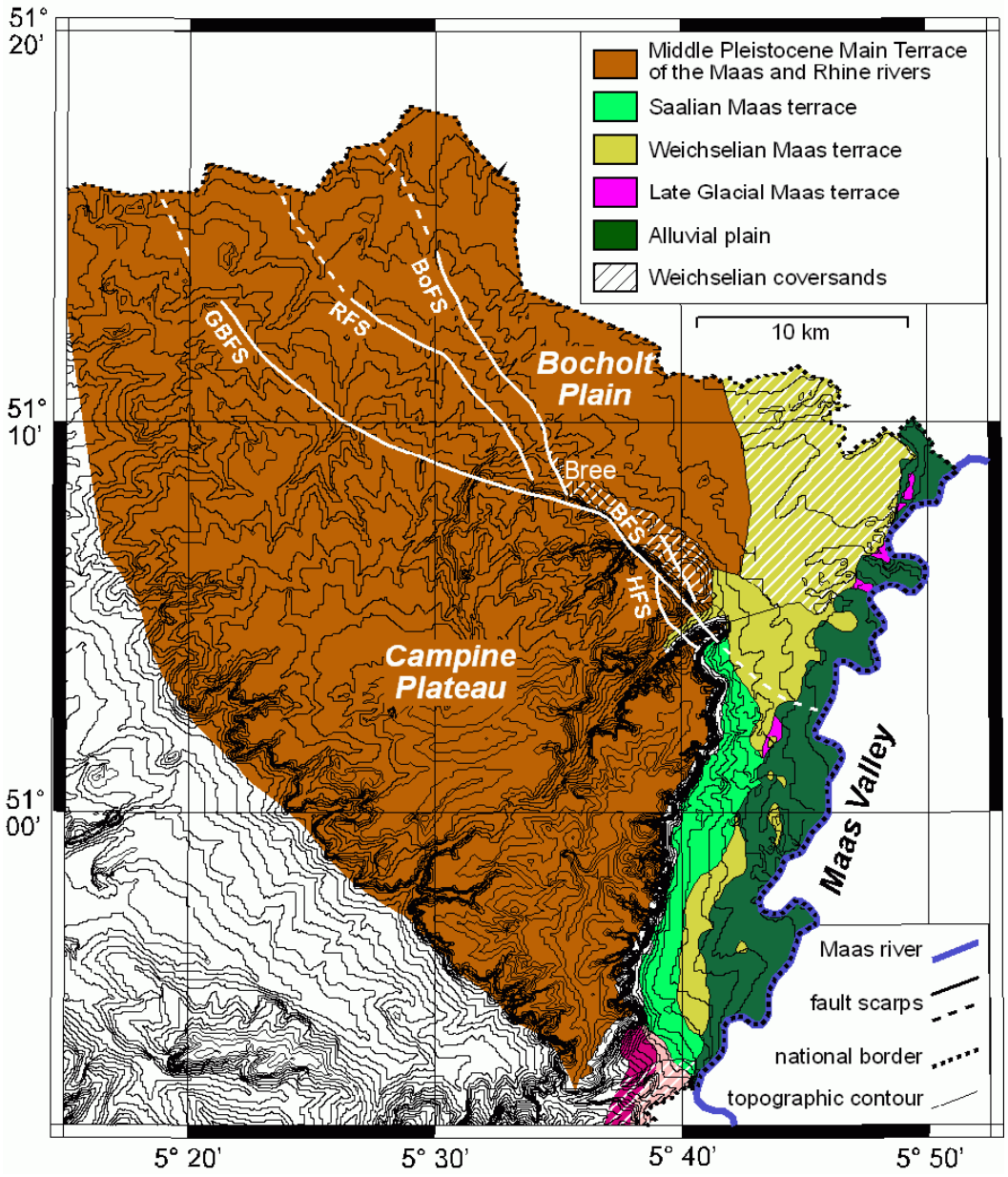

Fig. 27: Geomorphology of the Belgian part of the Roer graben area, showing position of fault scarps with respect to Middle and Late Pleistocene alluvial terraces (after Paulissen, 1973 and Paulissen, 1997). BFS = Bree fault scarp. Figure from Vanneste et al. (2001).

2.1. The Bree fault scarp

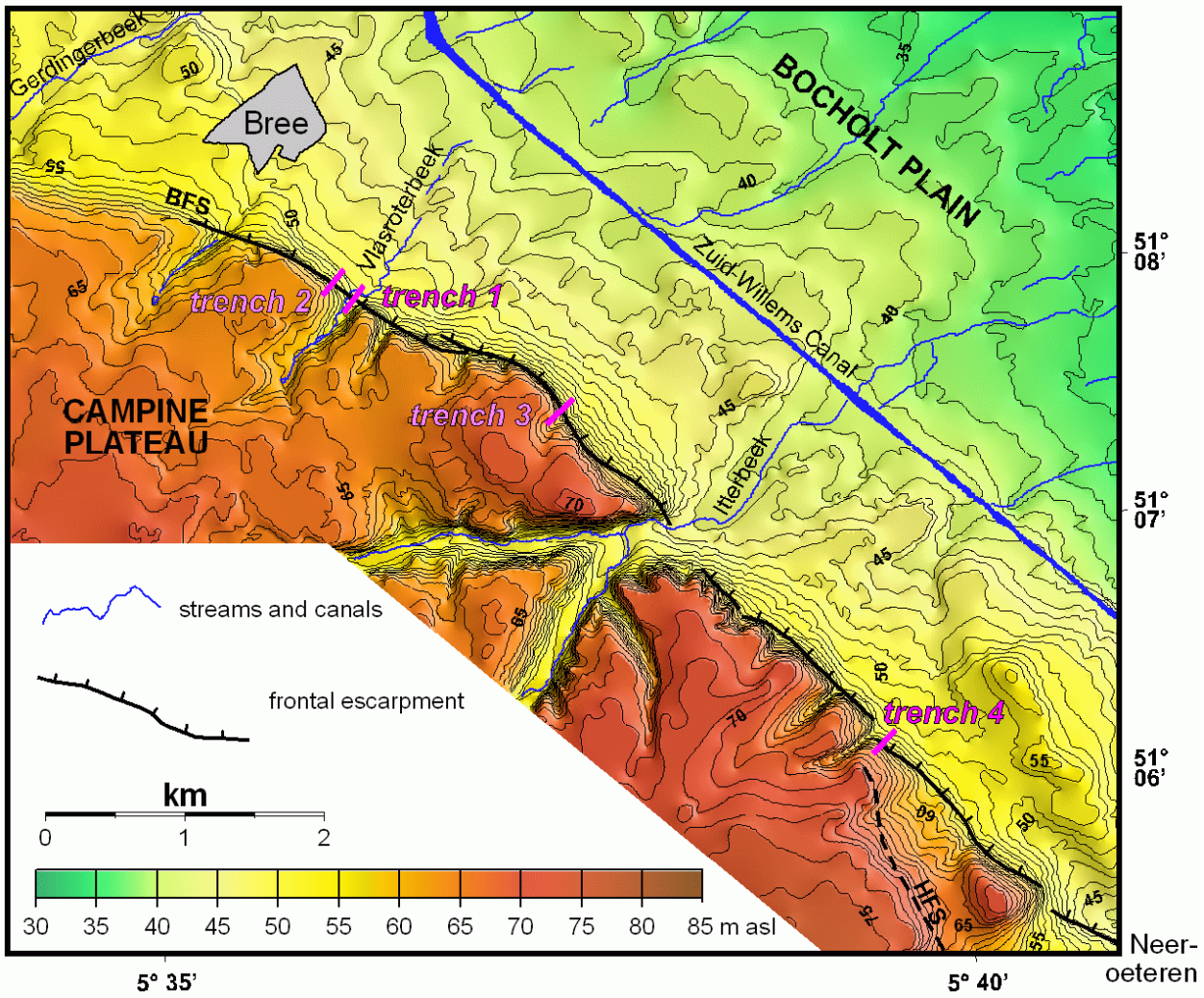

Fig. 28 DEM of the Bree fault scarp

Fig. 29: View of the Bree fault scarp in interfluvial position between Bree and Opitter

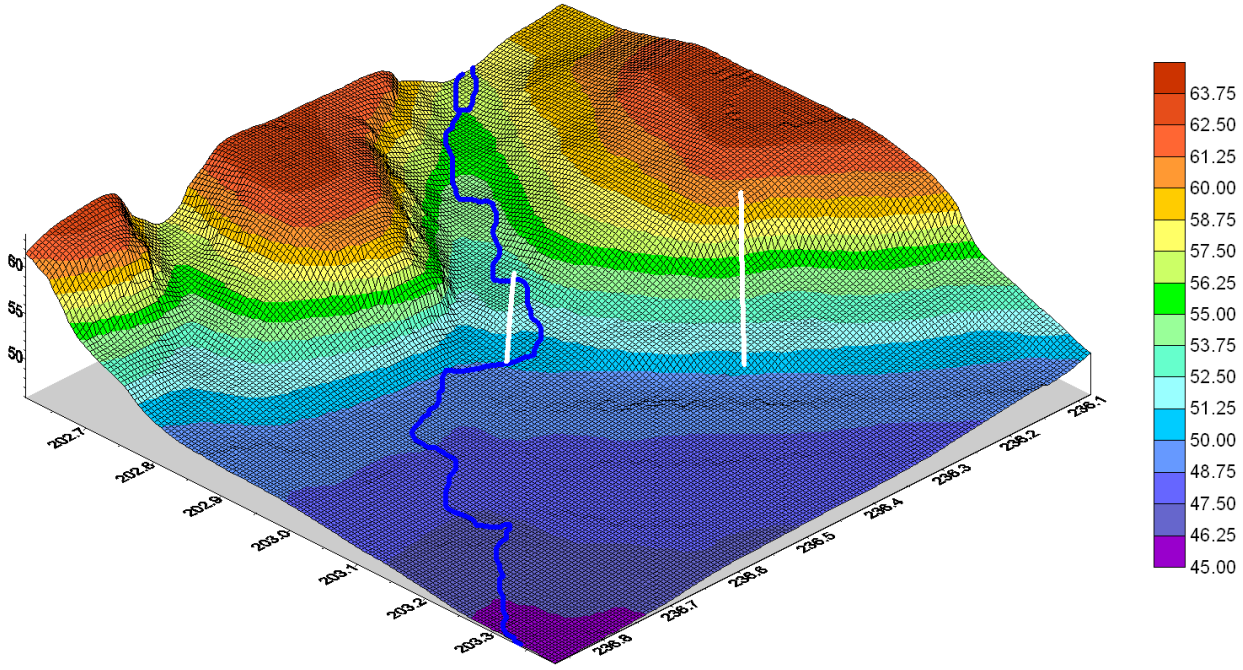

Fig. 30: DEM of trench sites 1 and 2 on the Bree fault scarp

Fig. 31: View of the scarplet at Bree trench site 1, situated in a small transverse valley across the Bree fault scarp.

Fig. 32: View of the fault zone in Bree trench 1.

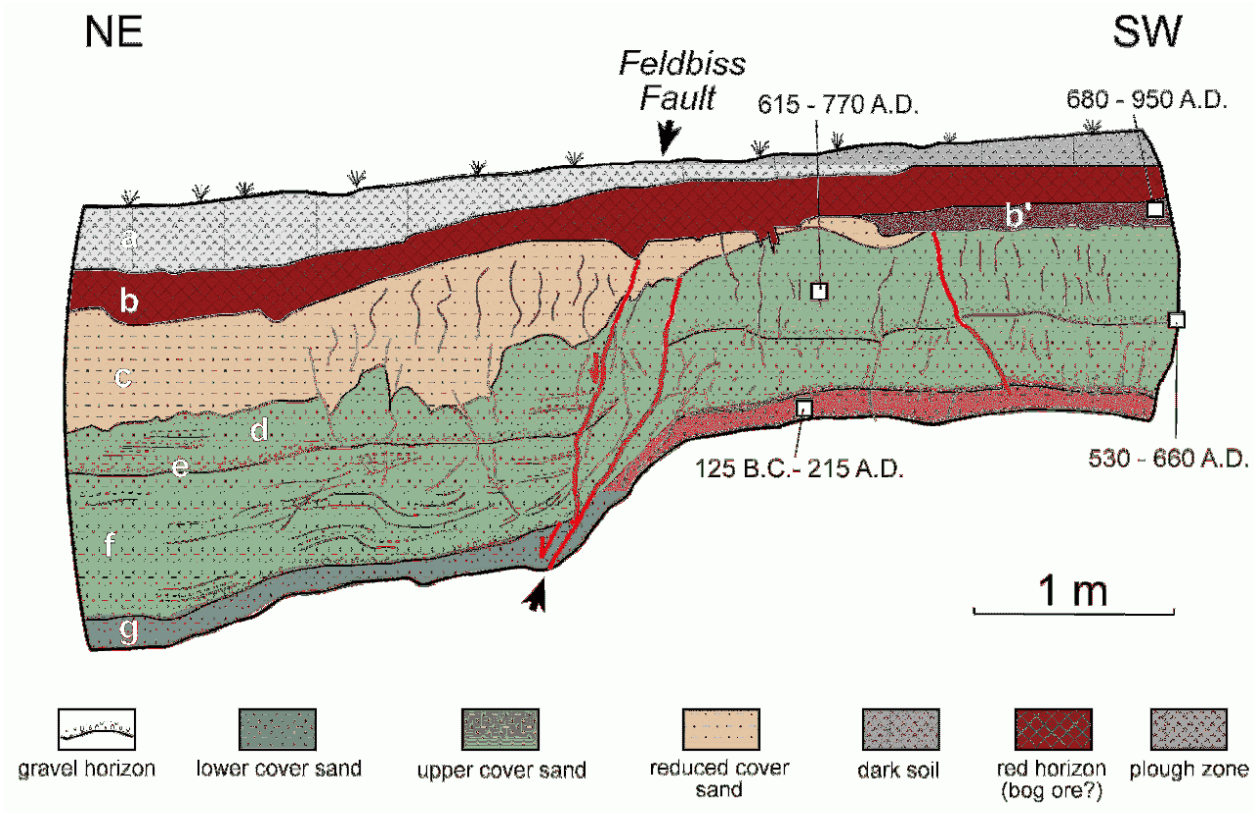

Fig. 33: Log of the central section of trench 1. Holocene soil c, which wedges out against the fault, has registered the last faulting event. The fault and fissures were subsequently penetrated by roots and covered by the b and b' units (brown and reddish soils). Calibrated radiocarbon dates of charcoal provide a time range for the last coseismic displacement between 610 AD and 890 AD. From Camelbeeck & Meghraoui (1998)

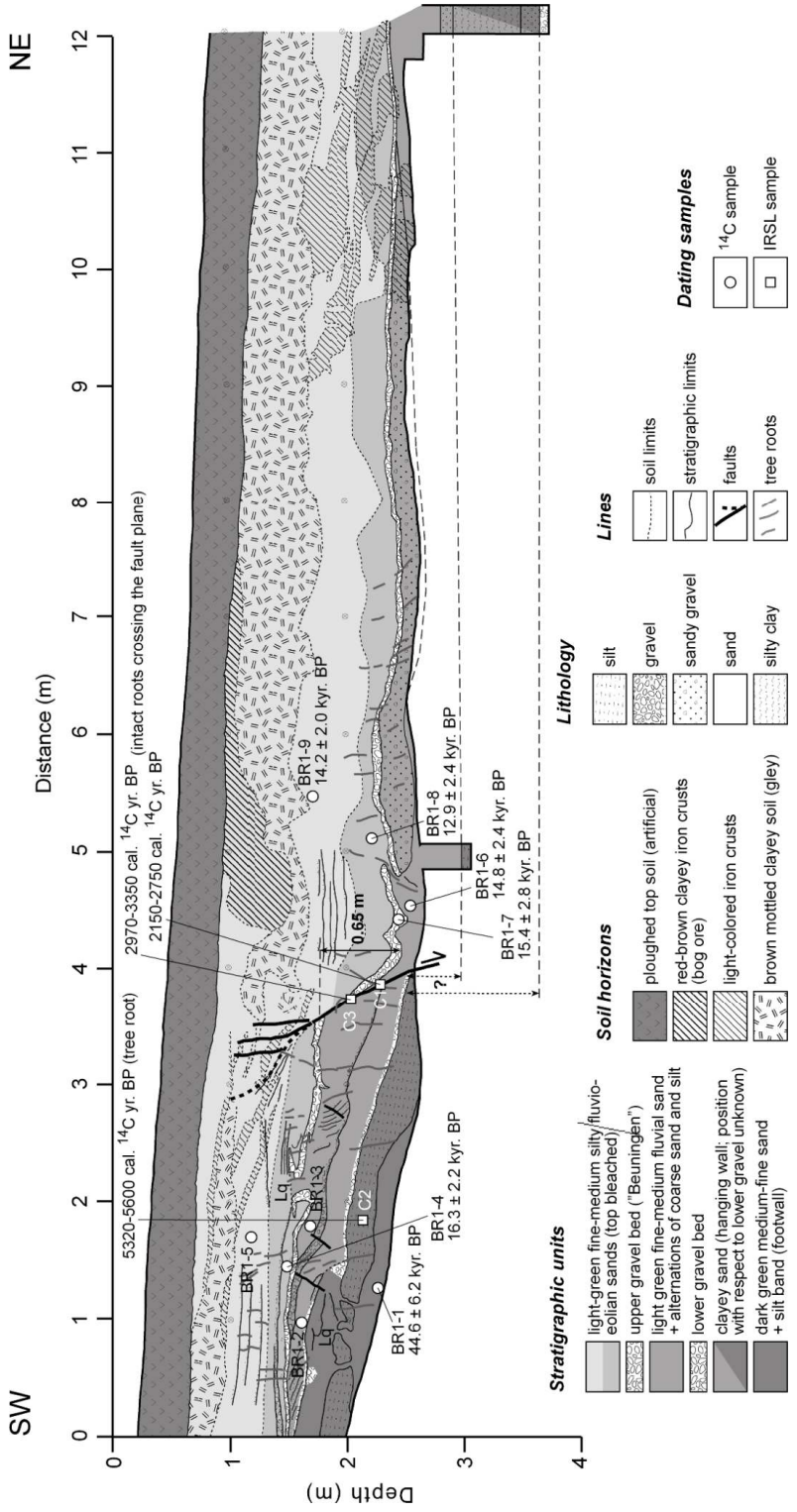

Fig. 34: Log of northwest wall of trench 1bis across the Bree fault scarp. One faulting event is evidenced by 0.65 m of vertical offset of a gravel bed that correlates with the regionally known "Beuningen" horizon dating back to the Last Glacial Maximum. Overlying late glacial fluvial-eolian sands, as well as the Holocene soil, are displaced by the same amount. The event horizon could not be identified, and it has most likely been destroyed by the artificial plough zone. Two plant roots crosscutting the fault plane and sealing fault movement were radiocarbon dated between 2150 and 3350 cal. yr B.P. A second event may be present just below the Beuningen horizon, but correlation between footwall and hanging wall is ambiguous and could not be verified because of the shallow water table. Infrared Stimulated Luminescence (IRSL) ages are from Frechen et al. (2001). Figure from Camelbeeck et al. (2007).

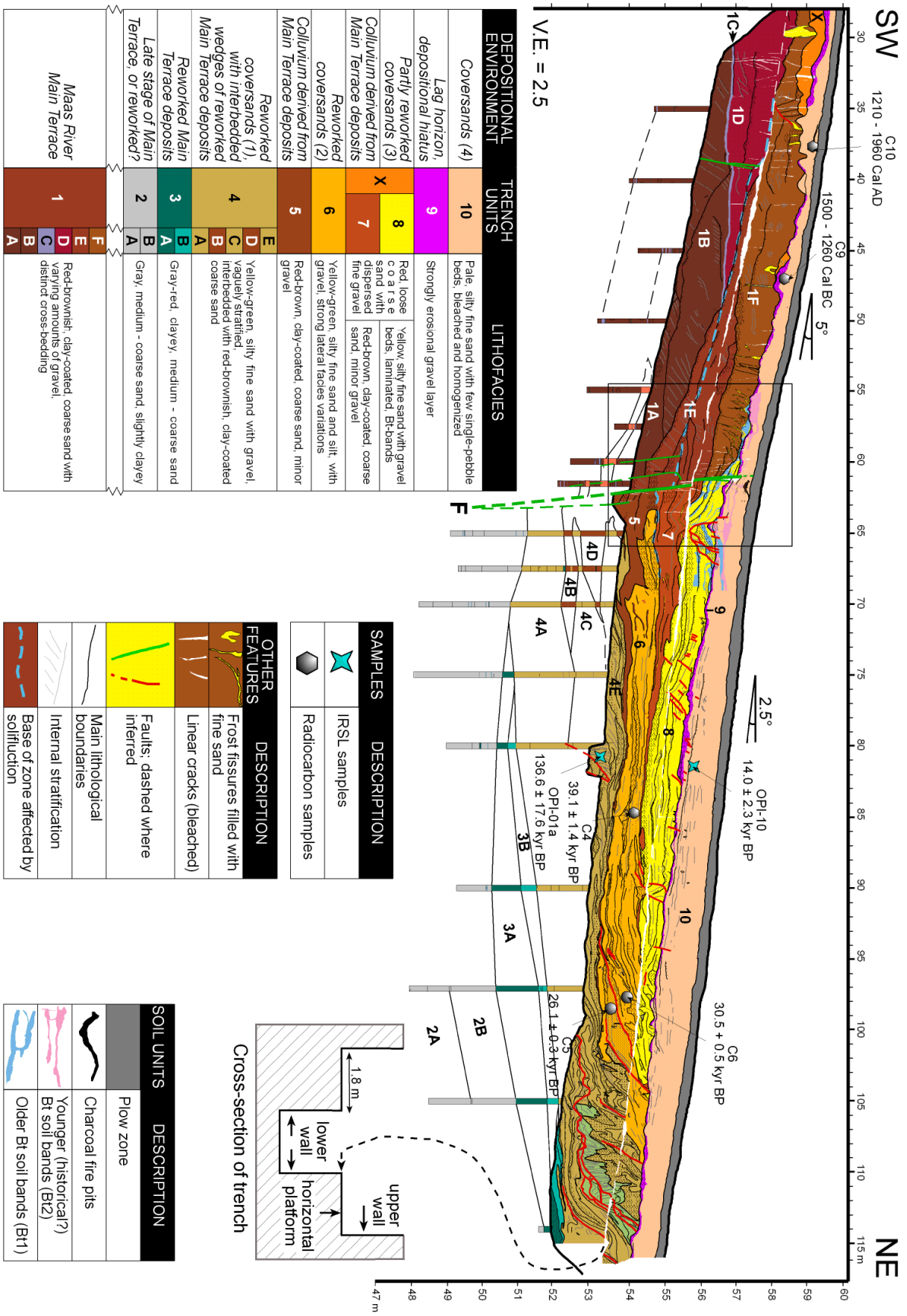

Fig. 35: Schematic drawing of northwest wall of trench 4 and stratigraphic summary. Note the break between lower and upper trench wall. Indicated are position of main fault (F), stratigraphic units (1–10) and dating results for samples outside fault zone. Vertical exaggeration is 2.5. Figure from Vanneste et al. (2001).

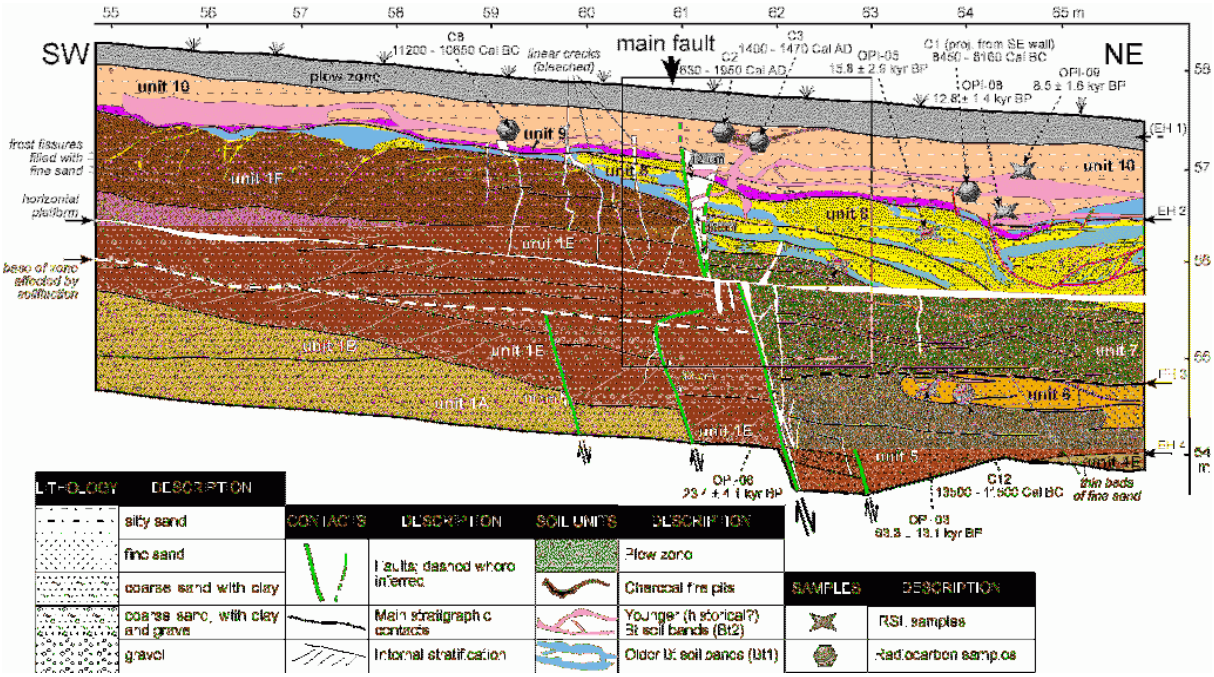

Fig. 36: Detailed log of main fault zone on northwest wall of trench 4, showing amount of displacement of correlative horizons, inferred position of event horizons (EH) and dating results. Thin, horizontal beds of fine sand within the wedge-shaped unit 7 in the hanging wall resemble bent frost fissures in footwall unit 1F. See Fig. 28 for location. Figure from Vanneste et al. (2001).

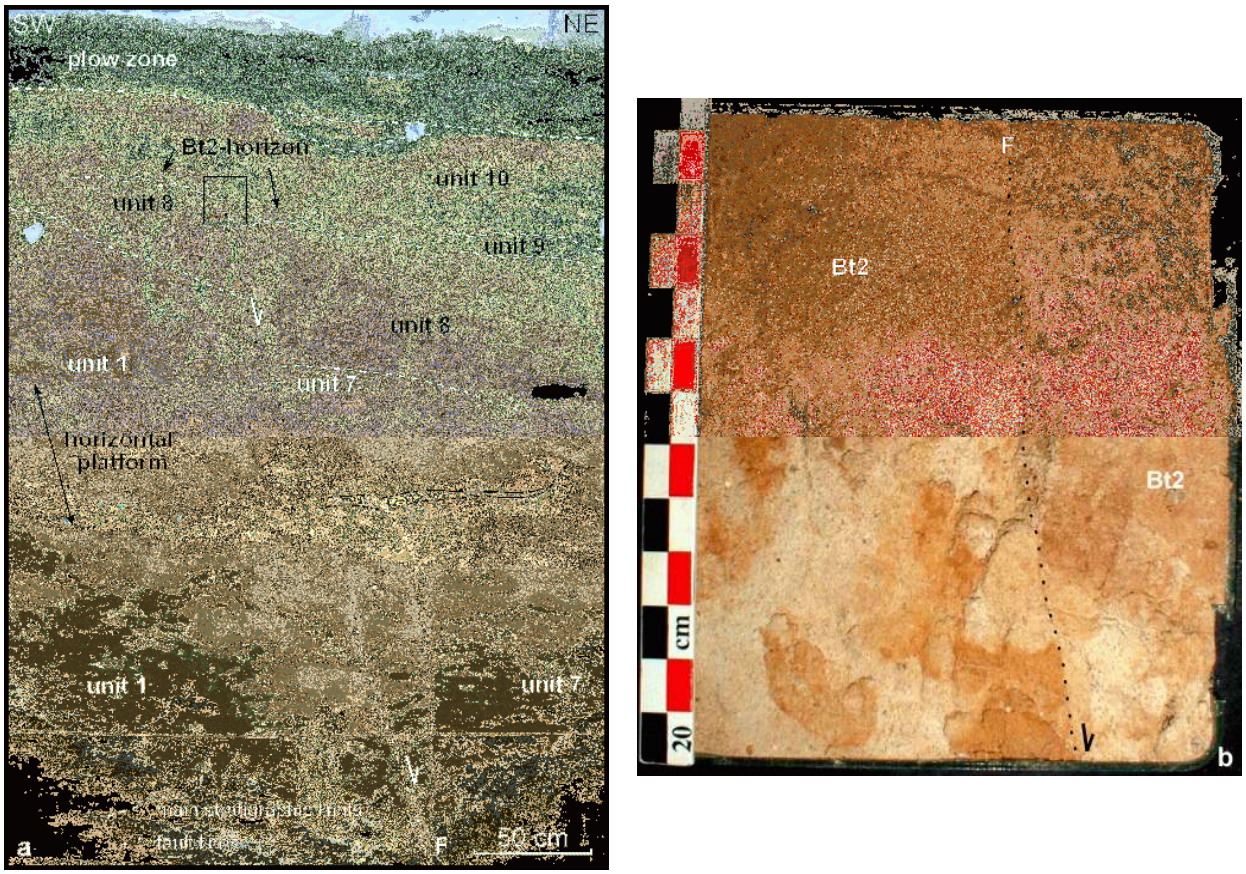

Fig. 37: Photographs of main fault on northwestern wall of trench 4: (a) expression of main fault (F) by displacement of correlative horizons (base of coversand unit 8, and gravel bed of unit 9) on upper trench wall, and as linear, bleached fissure on lower wall; black line on horizontal platform outlines position of laterally truncated frost fissure. Location is indicated in Fig. 36; (b) detail from box sample showing sharp vertical displacement of Bt2 soil horizon within unit 10. Dotted lines indicate position of main fault plane (F). Location corresponds approximately to rectangle in Fig. 37a. Figure from Vanneste et al. (2001).

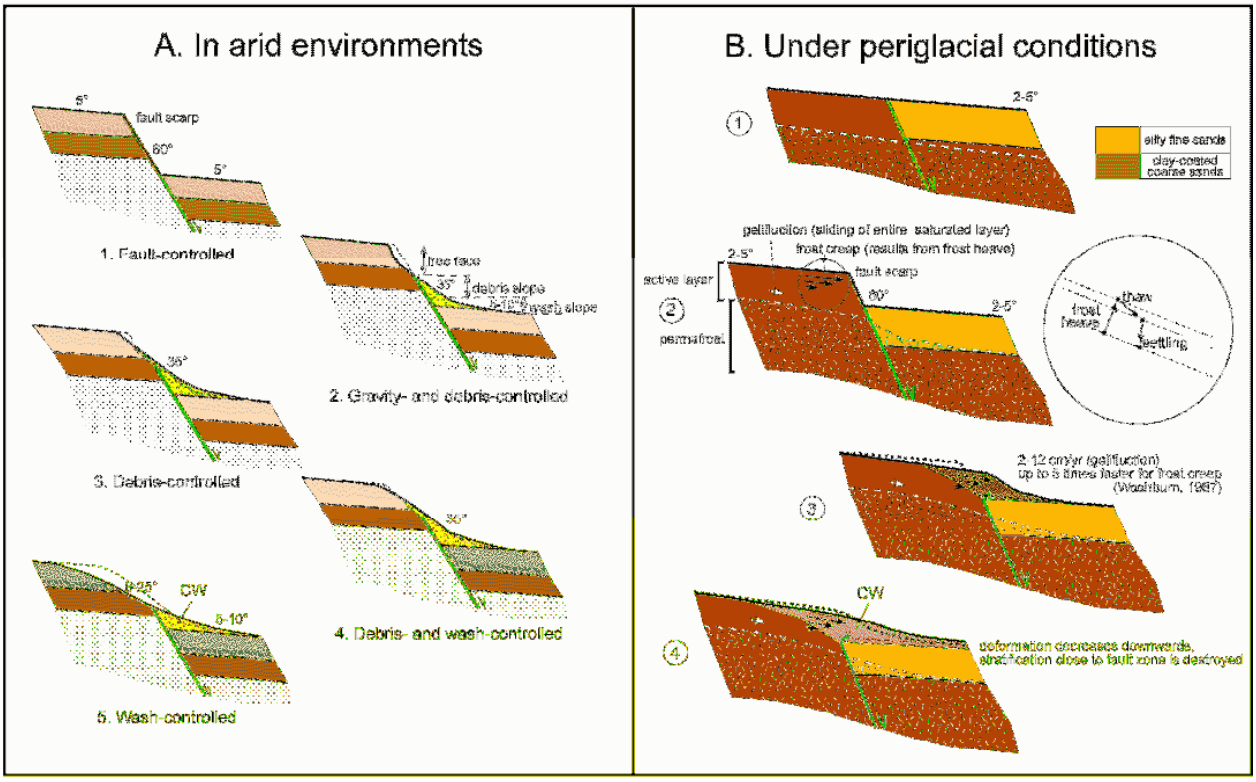

Fig. 38: Model for colluvial-wedge development following surface rupture in arid environments (Wallace, 1977) vs. under periglacial conditions at trench site 4. CW = colluvial wedge. Figure after Vanneste et al. (2001).

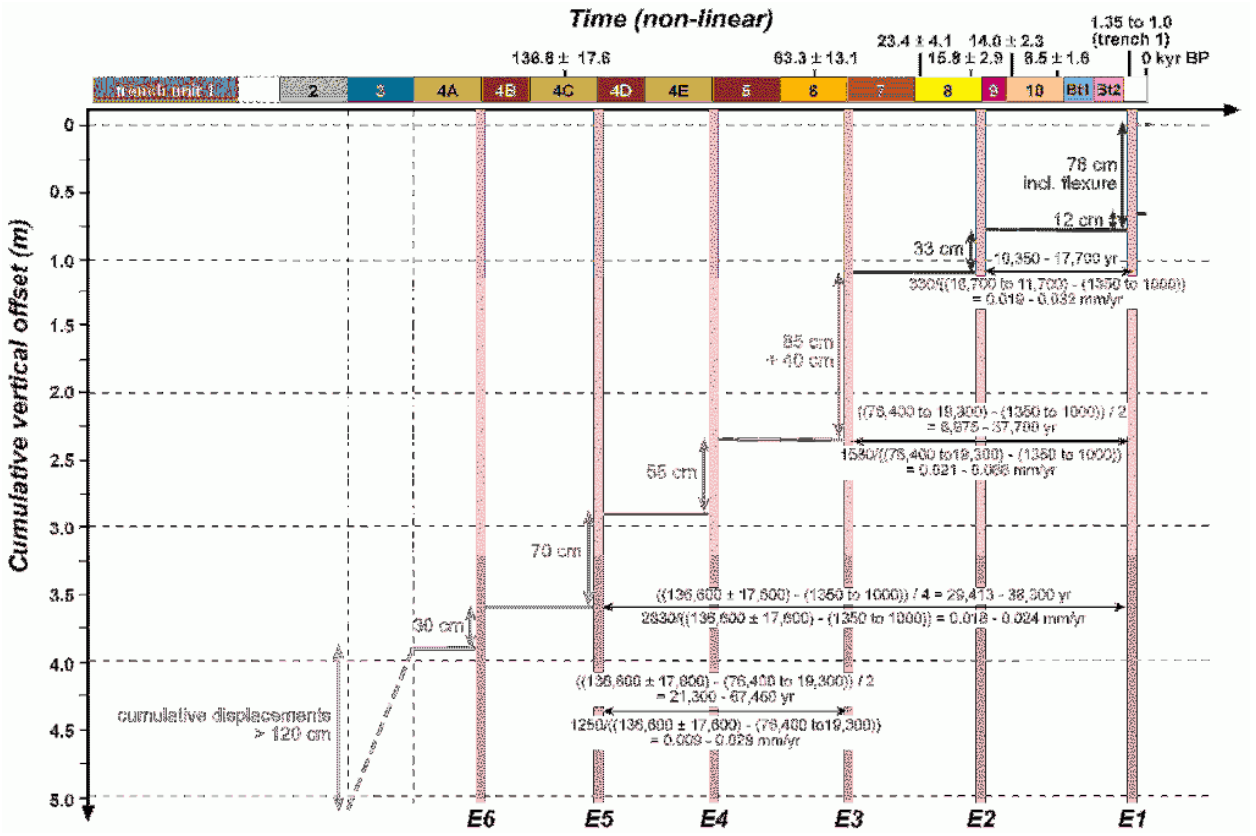

Fig. 39: Plot of cumulative amount of displacement produced by six paleoearthquakes on the Bree fault scarp versus time, based on data from trench site 4. Note that the time axis is expressed in stratigraphic units on which relevant dating results have been superposed and is thus not linear. The average return period and fault slip rate have been calculated for the earthquake cycles E5-E1, E5-E3, E3-E1, and E2-E1. Figure from Vanneste et al. (2001).

Paleo-earthquake	Trench 1	Trench 2	Trench 3	Trench 4	Correlation
Latest	0.5 m (fault slip) + 0.5 m (modeled flexure)	0.7 m (fault slip)	0.9 m (fault slip)	0.12 m (fault slip) + 0.7 m (modeled flexure)	0.55 m average displacement (0.85 m incl. flexure)
	> 1002 – 1272 yr. BP (^{14}C) [1] < 1181 – 1337 yr. BP (^{14}C) [1] In Trench 1bis: > 2970 – 3350 yr. BP (^{14}C) [7] < 12.9 ± 2.4 kyr. BP (IRSL) [6]	> 907 – 986 yr. BP (^{14}C) [1] < 2151 – 2342 yr. BP (^{14}C) [1]	< Older Coversand II (ca 13-10 kyr. BP) [8]	> 480 – 550 yr. BP (^{14}C) [4] < 10.11 – 10.40 kyr. BP (^{14}C) [4] < 6.8 ± 1.2 kyr. BP (IRSL) [5] < 2nd-generation Bt-soil fibre (historical?) [4]	(1337 – 1002 yr. BP) [1] 2970 – 8000 yr. BP
Penultimate		Lateral spreading, folding	0.5 m (fault slip)	0.33 m (fault slip)	0.4 m average displacement
		> Beuningen horizon (ca 19-14 kyr. BP) < 21.33 – 26.43 kyr. BP (^{14}C) [2]	≥ Beuningen horizon (ca 19-14 kyr. BP) [8] ≤ Older Coversand I (ca 27-22 kyr. BP) [8]	> Beuningen horizon > 11.4 ± 1.8 kyr. BP (IRSL) [5] < 12.0 ± 1.6 ka BP (IRSL) [5]	9.6 – 13.6 kyr. BP
Ante-penultimate		Soft-sediment deformation (folding)	1.2 m (fault slip)	0.85 + 0.40 m (fault slip)	1.2 m average displacement
		> 28.08 – 34.80 kyr. BP (^{14}C) [2]	> Older Coversand I (ca 27-22 kyr. BP) [8] < 44.79 ± 1.1 kyr. BP (^{14}C) [3]	> 22.2 ± 2.5 kyr. BP (IRSL) [5] < 69.0 ± 9.0 kyr. BP (IRSL) [5]	19.7 (28.08?) – 45.9 kyr. BP

Fig. 40: Correlation of paleoearthquakes (vertical displacement and dating) along the Bree fault scarp. From Camelbeeck et al. (2007).

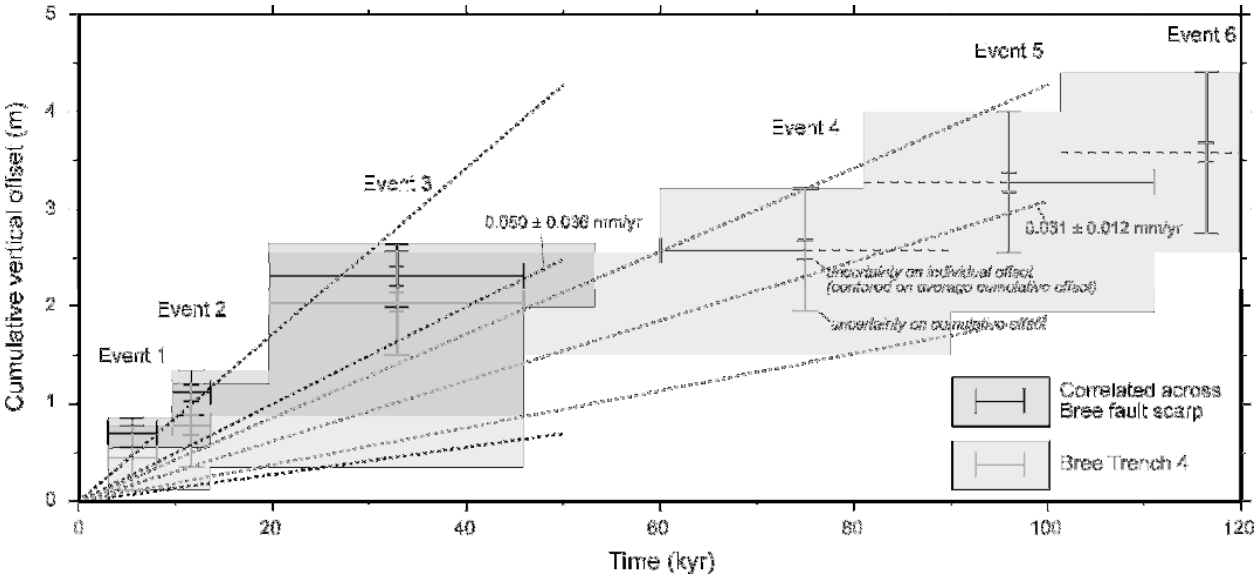

Fig. 41: Time-displacement diagram for paleoearthquakes along the Bree fault scarp. The diagram shows the envelope of time–cumulative offset solutions (incorporating their uncertainty) inferred from a correlation of the three most recent events (event 1 is the most recent) across all trenches (darker shade) and for the last six events identified in trench 4 (lighter shade). Superposed are average fault-slip rates (dotted lines) calculated from the last two and five complete earthquake cycles, respectively. Although the plot seems to suggest an increase of fault activity with time, the longer-term fault-slip rate falls entirely within the uncertainty limits of the shorter-term slip rate. From Camelbeeck et al. (2007).

2.2. The Geleen fault in the Belgian Maas River valley

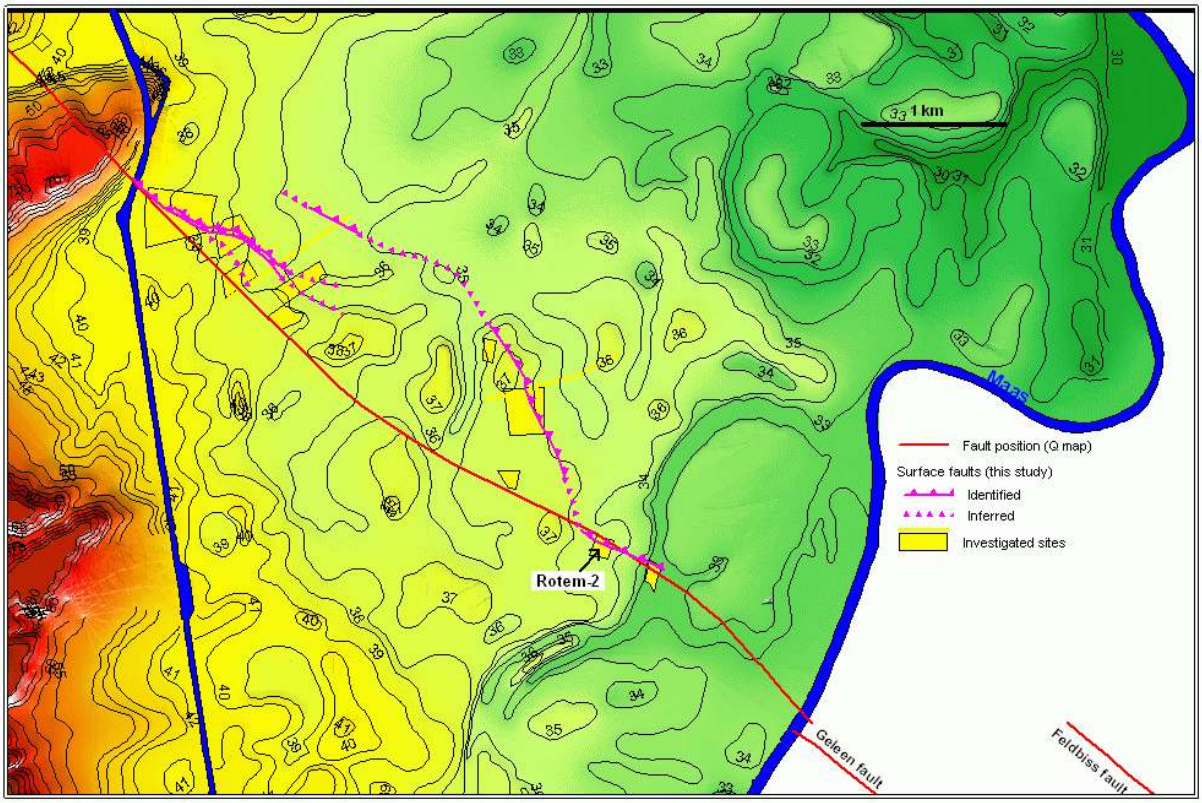

Fig. 42: Topography of the Belgian Maas River valley between Neeroeteren and Rotem, showing position of the Geleen fault according to the Quaternary geological map (red; Beerten et al., 1999), and as evidenced by geophysical surveying (pink, Vanneste et al., 2002).

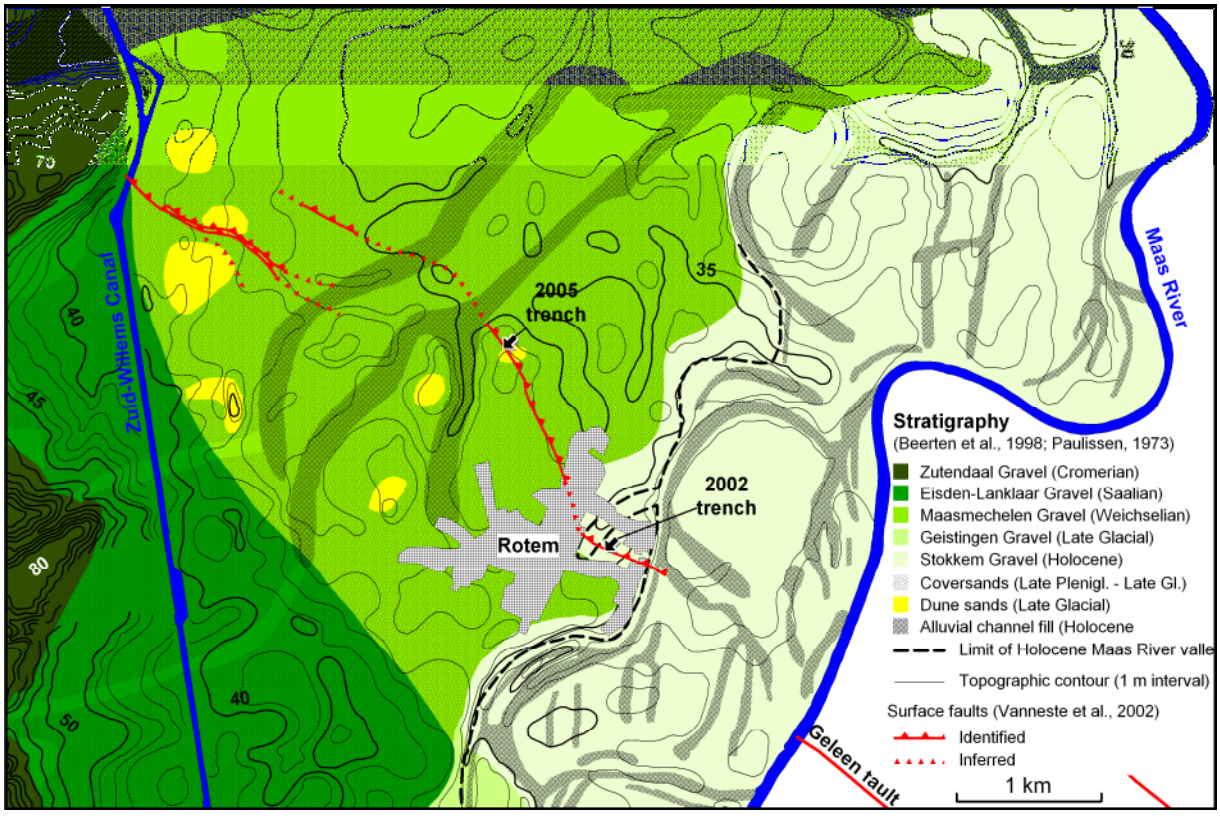

Fig. 43: Geomorphic map of the central portion of the Geleen fault in the Belgian Maas River valley, showing surface deposits (Paulissen, 1973; Beerten et al., 1998), the surface fault trace mapped from geophysical surveying (Vanneste et al., 2002), and the location of paleoseismic trenches excavated near Rotem in 2002 and 2005. From Vandenberghe et al. (2009).

Fig. 44: Aerial lineament and fault position from georadar north of Rotem

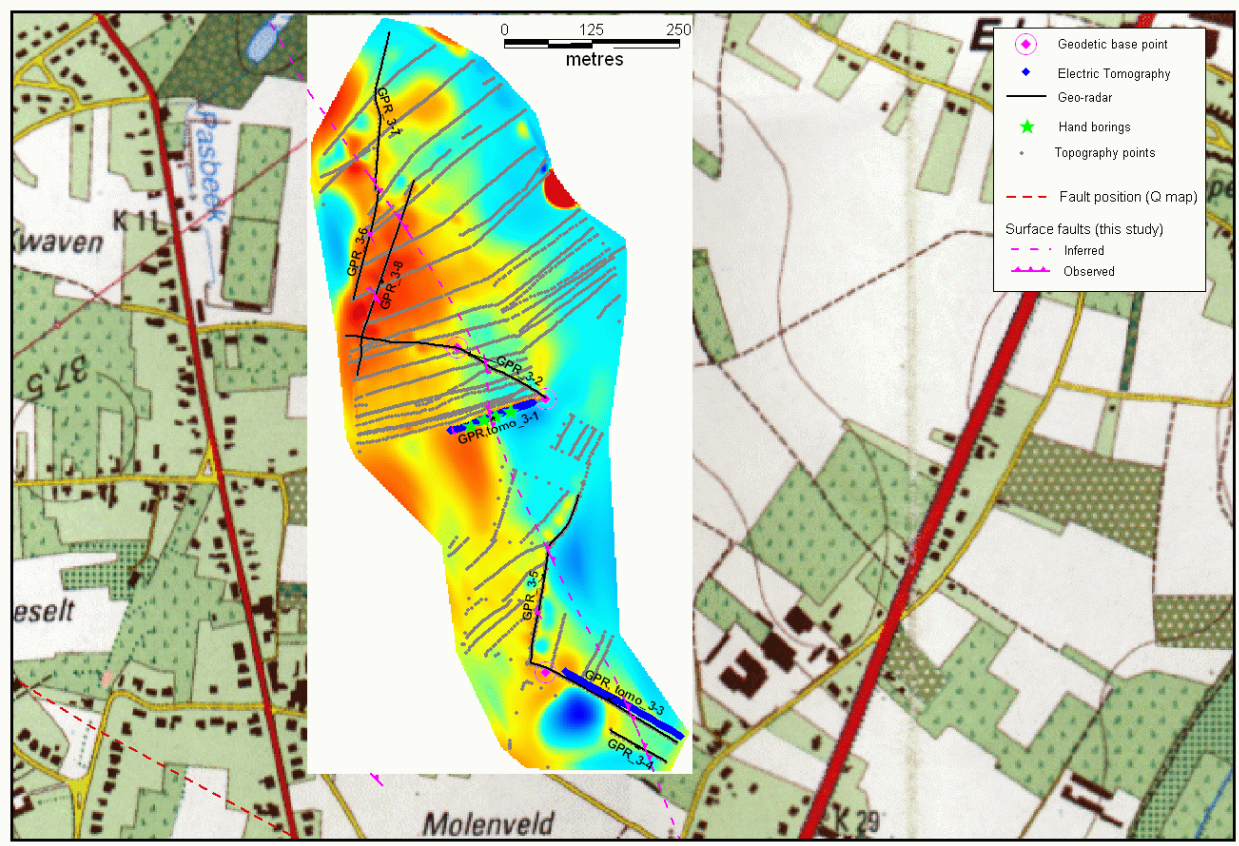

Fig. 45: DEM of area near Rotem-2005 trench site

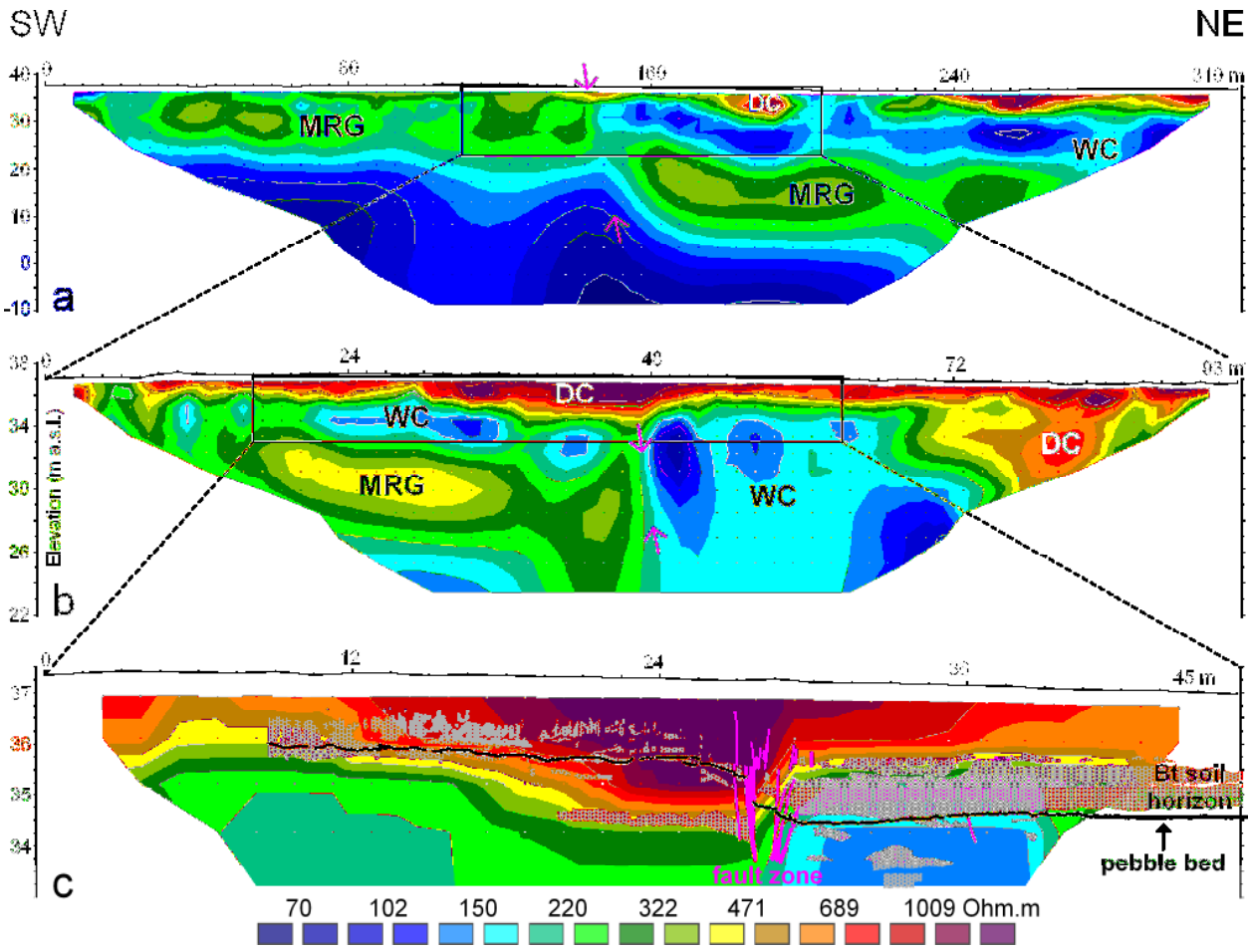

Fig. 46: a) ERT profile 1 (5-m electrode spacing, vertical exaggeration 1.25), showing 15 m of vertical offset at the base of an intermediate-resistivity layer interpreted as fluvial gravel (MRG=Maas River gravel). Pink arrows mark inferred fault position. b) ERT profile 2 (dE=1.5 m, VE=1.25), centered on the fault line identified from ERT profile 1. WC and DC denote wet and dry cover sands, respectively. Note apparent reverse displacement of DC at the fault. c) Resistivity-mapping profile 6 (dE=1.5 m, VE=2.0) along the axis of the later excavated trench with overlay of relevant stratigraphy, soil horizons, and fault splays mapped from the trench walls. The base of the high-resistivity layer appears to be controlled by the top of a clay-rich postdepositional soil (Bt horizon). Color scale is identical for all three profiles. Figure from Vanneste et al. (2008).

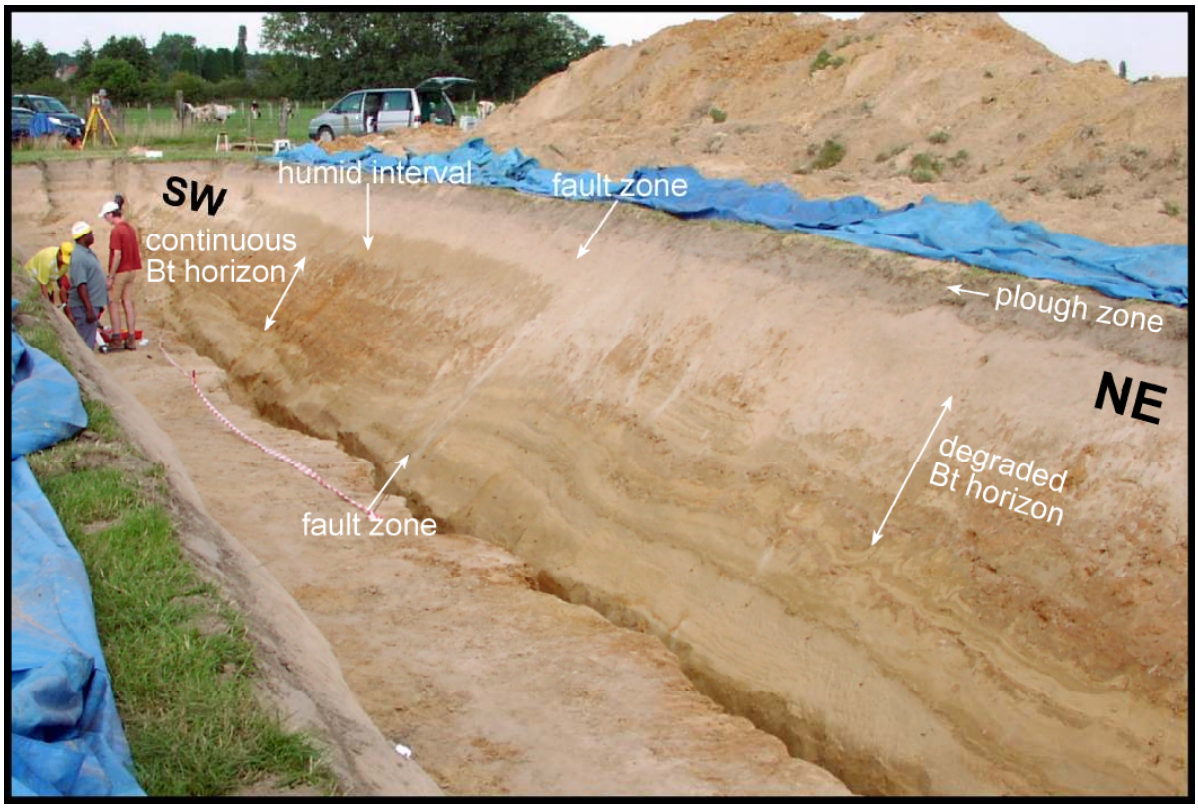

Fig. 47: Photo of inclined south-eastern wall of Rotem 2005 trench, showing vertically displaced Bt soil horizon. Note that the buried A horizon and overlying colluvium in the downthrown block cannot be distinguished in this lighting; the darker zone above the Bt horizon is due to a higher moisture content. Length and height of the trench wall are ca. 35 m and 3.5 m, respectively. Figure from Vanneste et al. (2008).

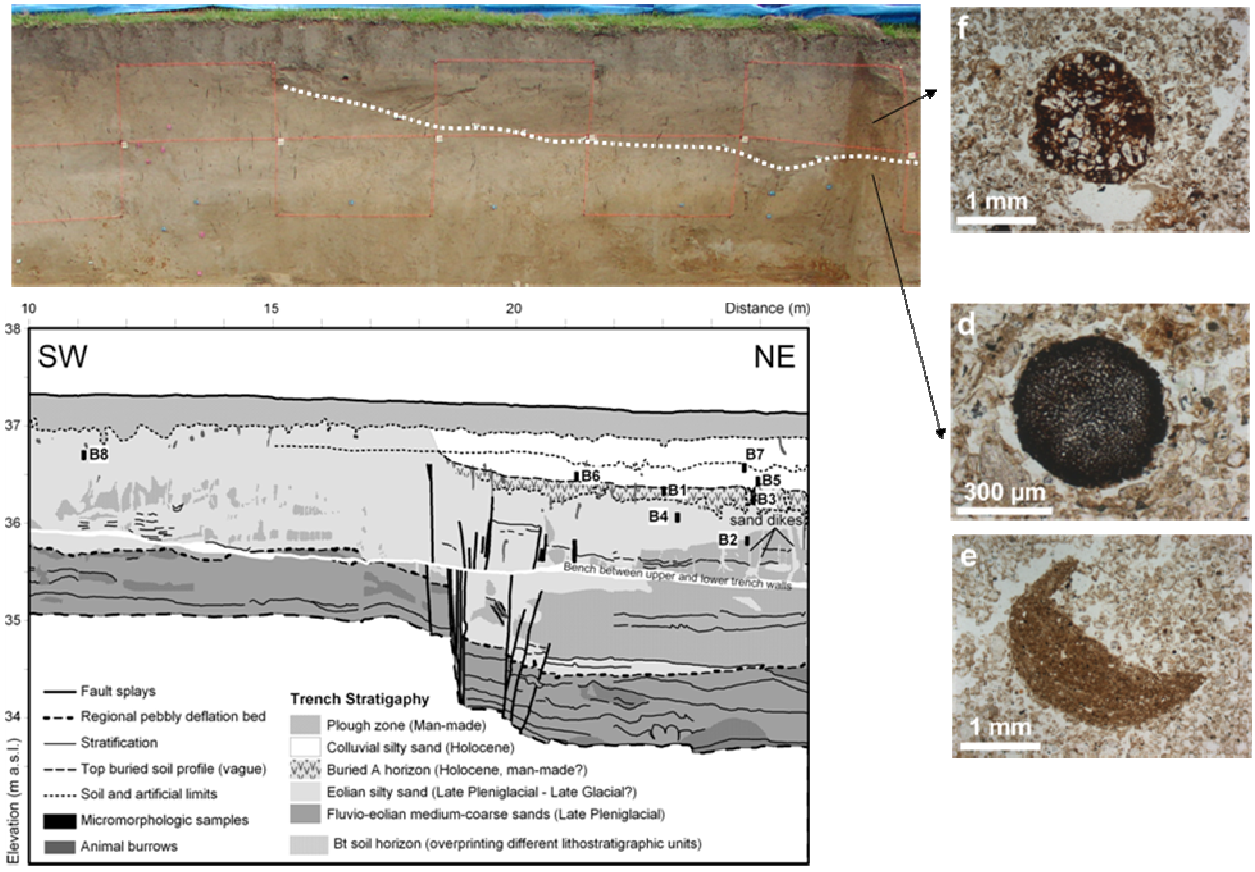

Fig. 48: Photo and simplified drawing of the fault zone on the NW wall of the Rotem 2005 trench. Thin sections indicate presence of colluvium above event horizon, and in situ soil below. Figure from Vanneste et al. (2008).

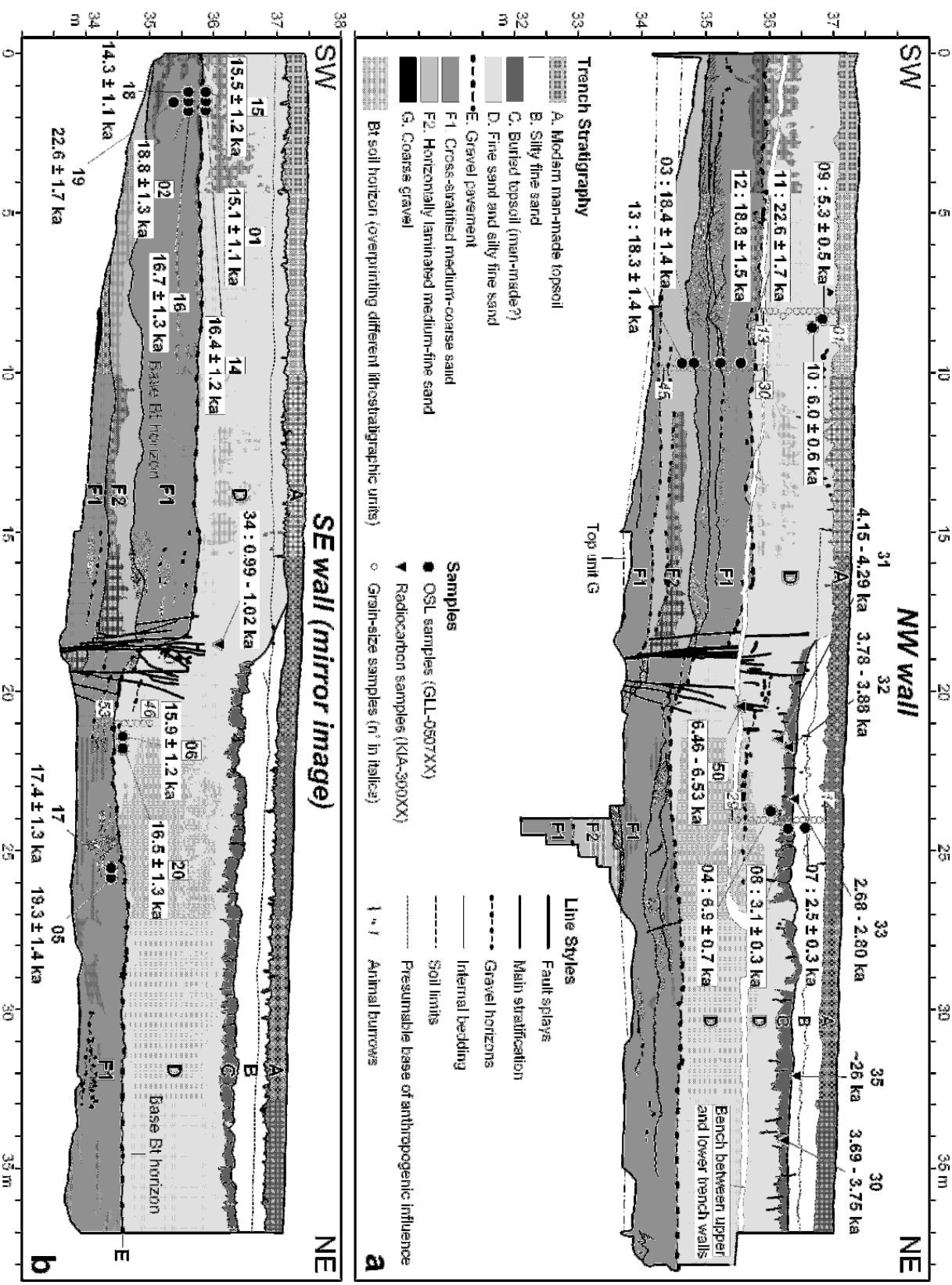

Fig. 49 – Simplified drawing of the sedimentary succession exposed on the walls of the trench excavated in 2005 across the Geleen fault near Rotem. The location and age of the 14C and OSL samples is indicated. All ages are expressed as ka before AD2005; the indicated 14C age refers to the range with the highest probability of the one-sigma calibration. Sample numbers refer to lab codes: (a) North-west wall (consisting of an upper and a lower vertical wall, separated by a horizontal bench); (b) South-east wall (continuous inclined wall). Each wall shows both sides of the fault. Figure taken from Vandenberghe et al. (2009).

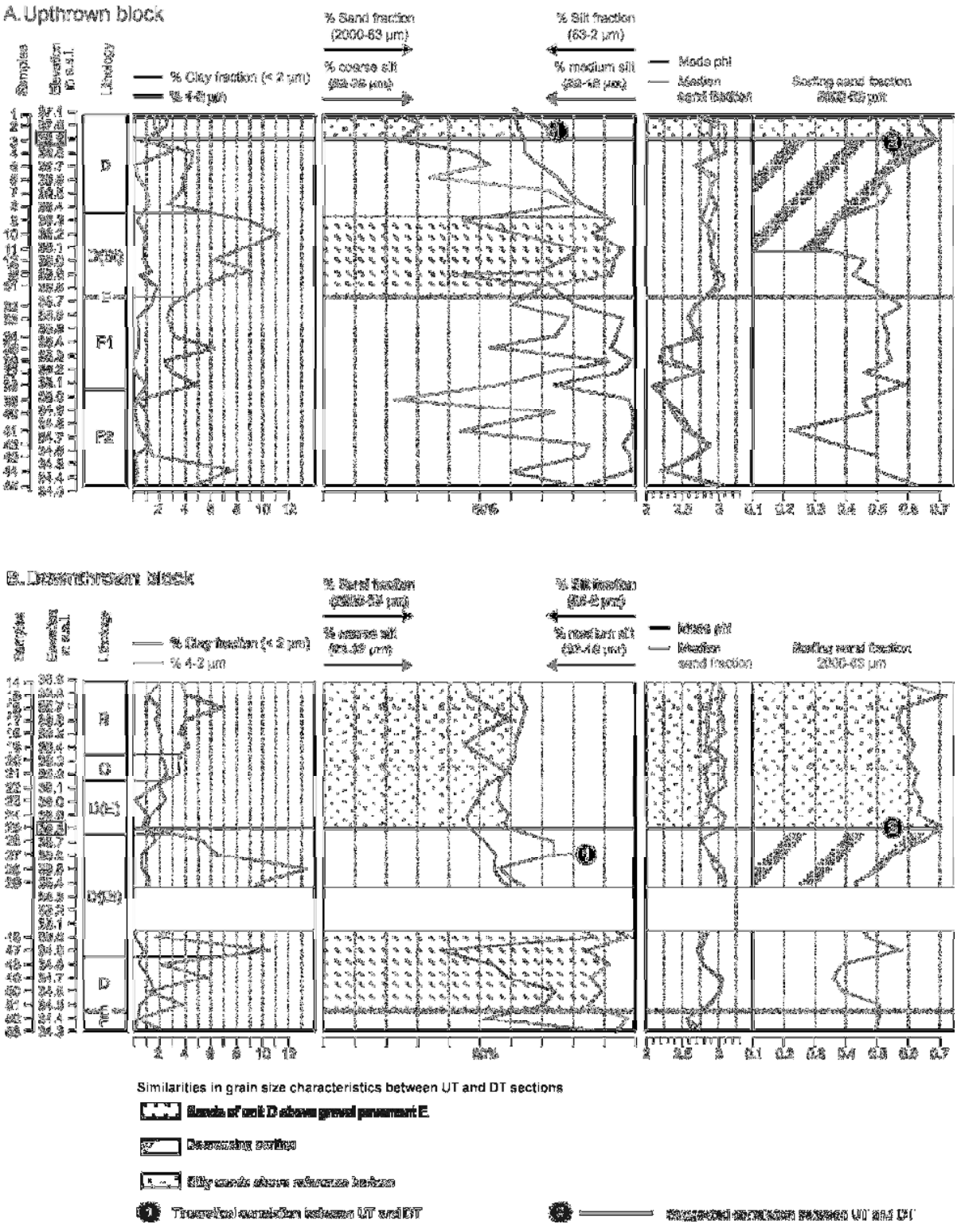

Fig. 50: Grain size characteristics of the sedimentary succession in the 2005 trench near Rotem. See Fig. 49 for sample position and legend lithology. Figure taken from Vandenberghe et al. (2009).

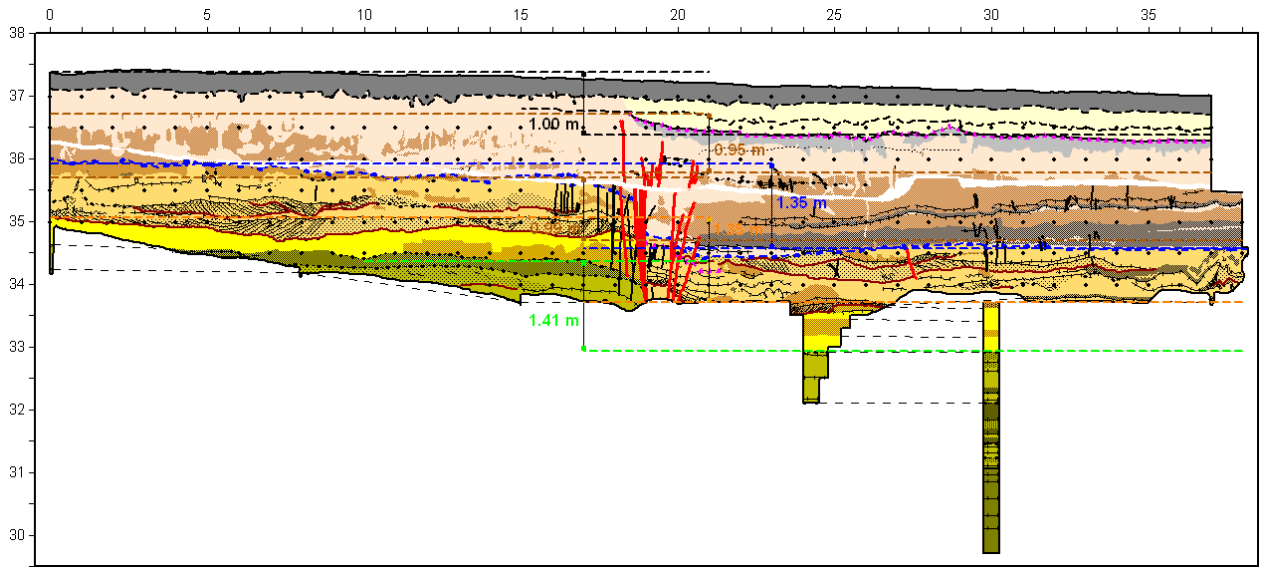

Fig. 51: Vertical offsets on SE wall of Rotem-2005 trench, showing two distinct groups, ~1.0 m and ~1.4 m, interpreted as evidence for two faulting events, a relatively young event with 1.0 m offset (pink event horizon), and an older event with 0.4 m offset (blue event horizon, = Beuningen pebble horizon).

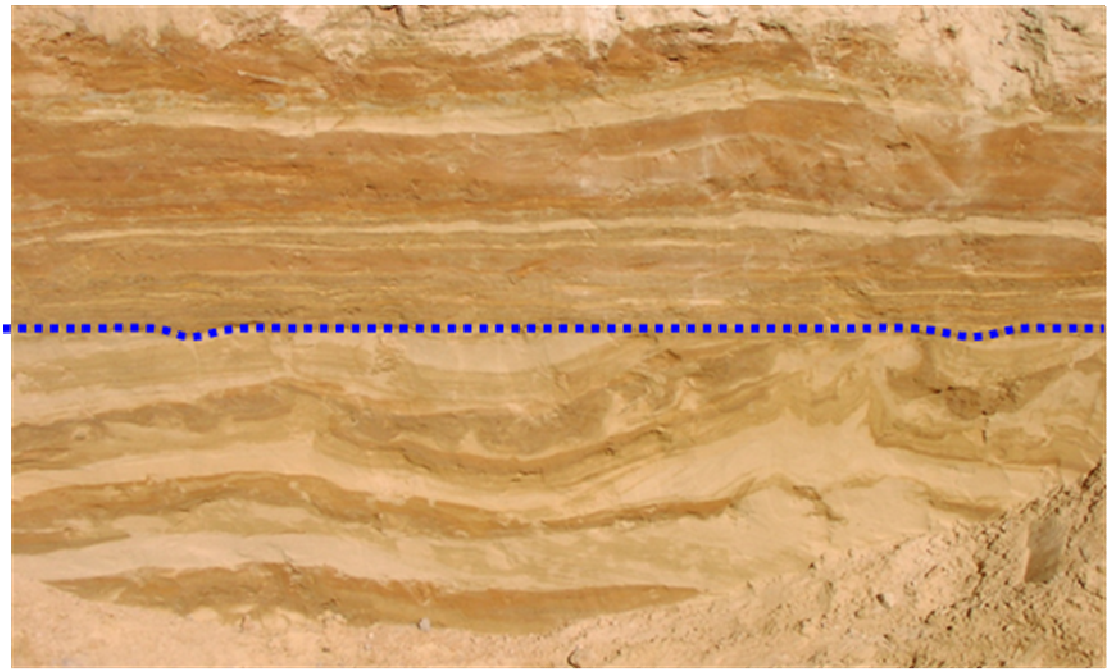

Fig. 52: Beuningen pebble bed truncating soft-sediment deformation features interpreted as co-seismic liquefaction in Rotem-2005 trench

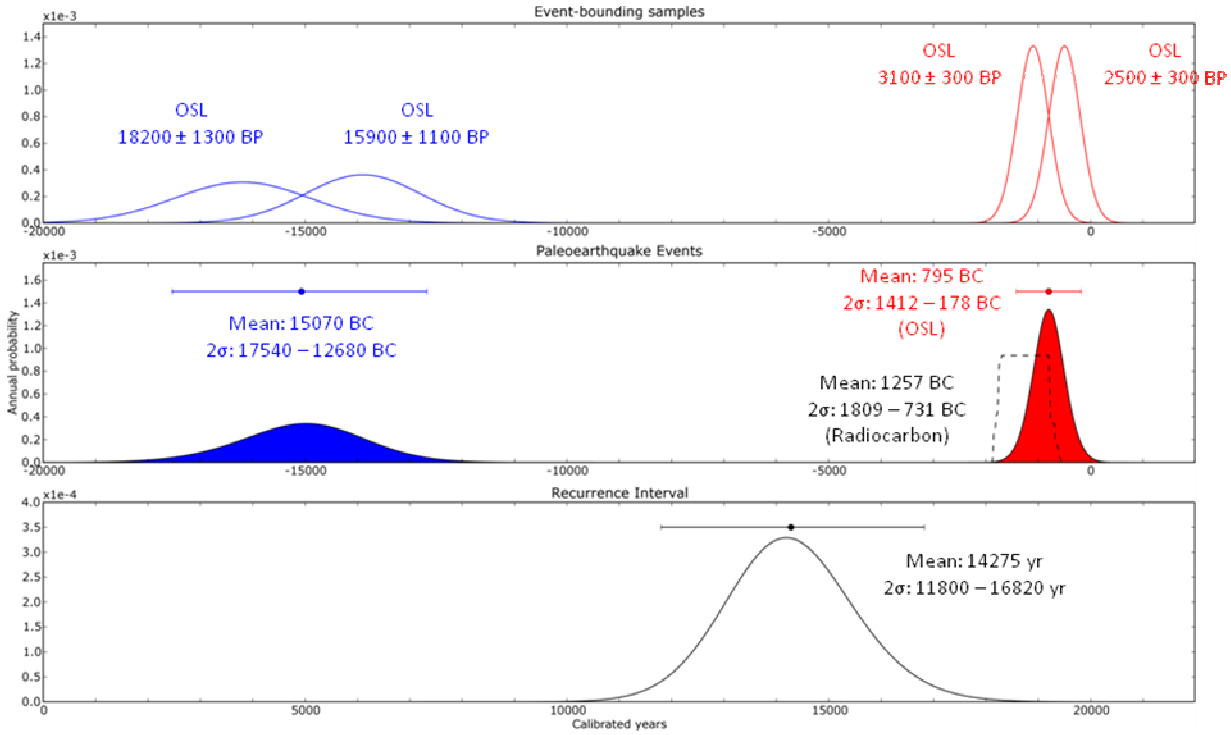

Fig. 53 – Summary of dating results in Rotem-2005 trench. Top: probability density distributions for event-bounding samples (OSL). Middle: probability density distributions for the two surface-rupturing events. Bottom: probability density distribution for the interval between both events.

Fig. 54 – Sand dikes evidencing coseismic liquefaction in Rotem-2005 trench (NW wall).

Fig. 55 – Gravel dike protruding from Late Weichselian Maas River gravel in Rotem-2002 trench.

Fig. 56– Photograph of northwestern wall of trench Rotem-2 in the Belgian Maas valley, showing the Geleen fault vertically displacing the top of the late Weichselian terrace and overlying eolian sands and silts by 0.75–1 m.

References

Beerten, K., Gullentops, F., Paulissen, E., Vandenberghe, N., 1998. Technisch verslag bij de Quartair kaart van België, Vlaams Gewest, Kaartblad Rekem (26). Administratie Natuurlijke Rijkdommen en Energie, Vlaamse Gemeenschap, Brussel.

Beerten, K., Brabers, P., Bosch, P. & Gullentops, F., 1998. The passage of the Feldbiss Bundle through the Maas Valley, *Aardkundige Mededelingen*, 9, 153-158.

Camelbeeck, T., Alexandre, P., Vanneste, K. & Meghraoui, M., 2000. Long-term seismicity in regions of present day low seismic activity: the example of western Europe, *Soil Dynamics and Earthquake Engineering,* 20**,** 405-414.

Camelbeeck, T., Martin, H., Vanneste, K., Verbeeck, K. & Meghraoui, M., 2001. Morphometric analysis of active normal faulting in slow-deformation areas: examples in the Lower Rhine Embayment, *Netherlands Journal of Geosciences / Geologie en Mijnbouw,* 80**,** 95-107.

Camelbeeck, T. & Meghraoui, M., 1996. Large earthquakes in northern Europe more likely than once thought, *EOS, Transactions, AGU,* 77**,** 405,409.

Camelbeeck, T. & Meghraoui, M., 1998. Geological and geophysical evidence for large paleoearthquakes with surface faulting in the Roer Graben (northwest Europe), *Geophysical Journal International,* 132**,** 347-362.

Camelbeeck, T., Vanneste, K., Alexandre, P., Verbeeck, K., Petermans, T., Rosset, P., Everaerts, M., Warnant, M. & Van Camp, M., 2007. Relevance of active faulting and seismicity studies to assessments of long-term earthquake activity and maximum magnitude in intraplate northwest Europe, between the Lower Rhine Embayment and the North Sea *in Continental Intraplate Earthquakes: Science, Hazard, and Policy Issues*, pp. 193-224, eds. Stein, S. & Mazzotti, S. Geological Society of America.

Demanet, D., Renardy, F., Vanneste, K., Jongmans, D., Camelbeeck, T. & Meghraoui, M., 2001. The use of geophysical prospecting for imaging active faults in the Roer graben, Belgium, *Geophysics,* 66**,** 78-89.

Demyttenaere, R., 1988, De Post-Paleozoïsche geologische geschiedenis van Noord-België, Unpublished Ph.D. thesis, K.U.Leuven.

De Ridder N.A., 1959, De kwartaire en de jongtertiaire tektoniek van Midden-Limburg en ZE-N Brabant, *Geologie en Mijnbouw*, 21, 1-24.

Felder, W.M., Bosch, P.W., Bisschops, J.H., 1989. Geologische kaart van Zuid-Limburg en omgeving, schaal 1:50000, Afzettingen van de Maas, Rijks Geologische Dienst, Haarlem.

Frechen, M., Vanneste, K., Verbeeck, K., Paulissen, E. & Camelbeeck, T., 2001. The deposition history of the coversands along the Bree Fault Escarpment, NE Belgium, *Netherlands Journal of Geosciences / Geologie en Mijnbouw,* 80**,** 171-185.

Geluk, M.C., Duin, E.J.TH., Dusar, M., Rijkers, R.H.B., Van den berg, M.W. & Van Rooijen, P;, 1994, Stratigraphy and tectonics of the Roer Valley Graben, Geologie en Mijnbouw, 73, 129-141.

Meghraoui, M., Camelbeeck, T., Vanneste, K., Brondeel, M. & Jongmans, D., 2000. Active faulting and paleoseismology along the Bree Fault Zone, Lower Rhine Graben (Belgium), *Journal of Geophysical Research,* 105**,** 13809-13841.

Paulissen, E., 1973. De Morfologie en Kwartairstratigrafie van de Maasvallei in Belgisch Limburg. Verh. Kon. Acad. Wetensch., Letteren en Schone Kunsten v. België, Kl. der Wetensch., vol. 127, 266pp (in Dutch).

Paulissen, E., 1983. Les nappes alluviales et les failles quaternaires du Plateau de Campine, in : Robaszynski, F. & Dupuis, Ch. (Eds.) Guides Géologiques Régionaux : Belqique, 167-170.

Paulissen, E., 1997. Quaternary morphotectonics in the belgian part of the Roer Graben. Belgian Symposium on Structural Geology and tectonics, *Aardkundige Mededelingen*, 8, 131-134.

Paulissen, E., Vandenberghe, J. and Gullentops, F., 1985, The Feldbiss fault in the Mass valley bottom (Limburg, Belgium), *Geologie en Mijnbouw*, 64, 79-87.

Van den Berg, M., Vanneste, K., Dost, B., Lokhorst, A., van Eijk, M. & Verbeeck, K., 2002. Paleoseismic investigations along the Peel Boundary Fault: geological setting, site selection and trenching results, *Netherlands Journal of Geosciences / Geologie en Mijnbouw,* 81**,** 39-60.

Vandenberghe, D., Vanneste, K., Verbeeck, K., Paulissen, E., Buylaert, J.-P., De Corte, F. & Van den haute, P., 2009. Late Weichselian and Holocene earthquake events along the Geleen fault in NE Belgium: OSL age constraints, *Quaternary International,* 199, 56-74.

Vanneste, K., Mees, F. & Verbeeck, K., 2008. Thin-section analysis as a tool to aid identification of palaeoearthquakes on the “slow”, active Geleen Fault, Roer Valley Graben, *Tectonophysics,* 453**,** 94-109.

Vanneste, K., Meghraoui, M. & Camelbeeck, T., 1999. Late Quaternary earthquake-related soft-sediment deformation along the Belgian portion of the Feldbiss Fault, Lower Rhine Graben system, *Tectonophysics,* 309**,** 57-79.

Vanneste, K. & Verbeeck, K., 2001. Paleoseismological analysis of the Rurrand fault near Jülich, Roer Valley graben, Germany: Coseismic or aseismic faulting history?, *Netherlands Journal of Geosciences / Geologie en Mijnbouw,* 80**,** 155-169.

Vanneste, K., Verbeeck, K. & Camelbeeck, T., 2002. Exploring the Belgian Maas valley between Neeroeteren and Bichterweert for evidence of active faulting, *Aardkundige Mededelingen,* 12**,** 5-8.

Vanneste, K., Verbeeck, K. & Camelbeeck, T., 2008. A decade of paleoseismic research in the Roer Valley graben. *in Seismic risk: Earthquakes in North-Western Europe*, pp. 57-64, eds Camelbeeck, T., Degée, H., Degrande, G. & Sabbe, A. éditions de l'Université de Liège, Liège.

Vanneste, K., Verbeeck, K., Camelbeeck, T., Paulissen, E., Meghraoui, M., Renardy, F., Jongmans, D. & Frechen, M., 2001. Surface-rupturing history of the Bree fault scarp, Roer Valley graben: Evidence for six events since the late Pleistocene, *Journal of Seismology,* 5**,** 329-359.

Vanneste, K., Verbeeck, K. & Petermans, T., 2008. Pseudo-3D imaging of a low-slip-rate, active normal fault using shallow geophysical methods: The Geleen fault in the Belgian Maas River valley, *Geophysics,* 73**,** B1-B9.

PDF: http://seismologie.oma.be/active.php?LANG=NL&CNT=BE&LEVEL=1600

3. Stop 3 Opgrimbie - Type Section

Topics: - Stratigraphy of the Last Termination
- Phases of Aeolian activity
- Wild fires during the Alleröd

By E. Paulissen, C. Derese and P. Van den haute

Pictures taken in 1968: two bleached horizons (the Usselo soil and the Opgrimbie soil) grading into two superposed organic layers.

The two organic layers cored on 090428

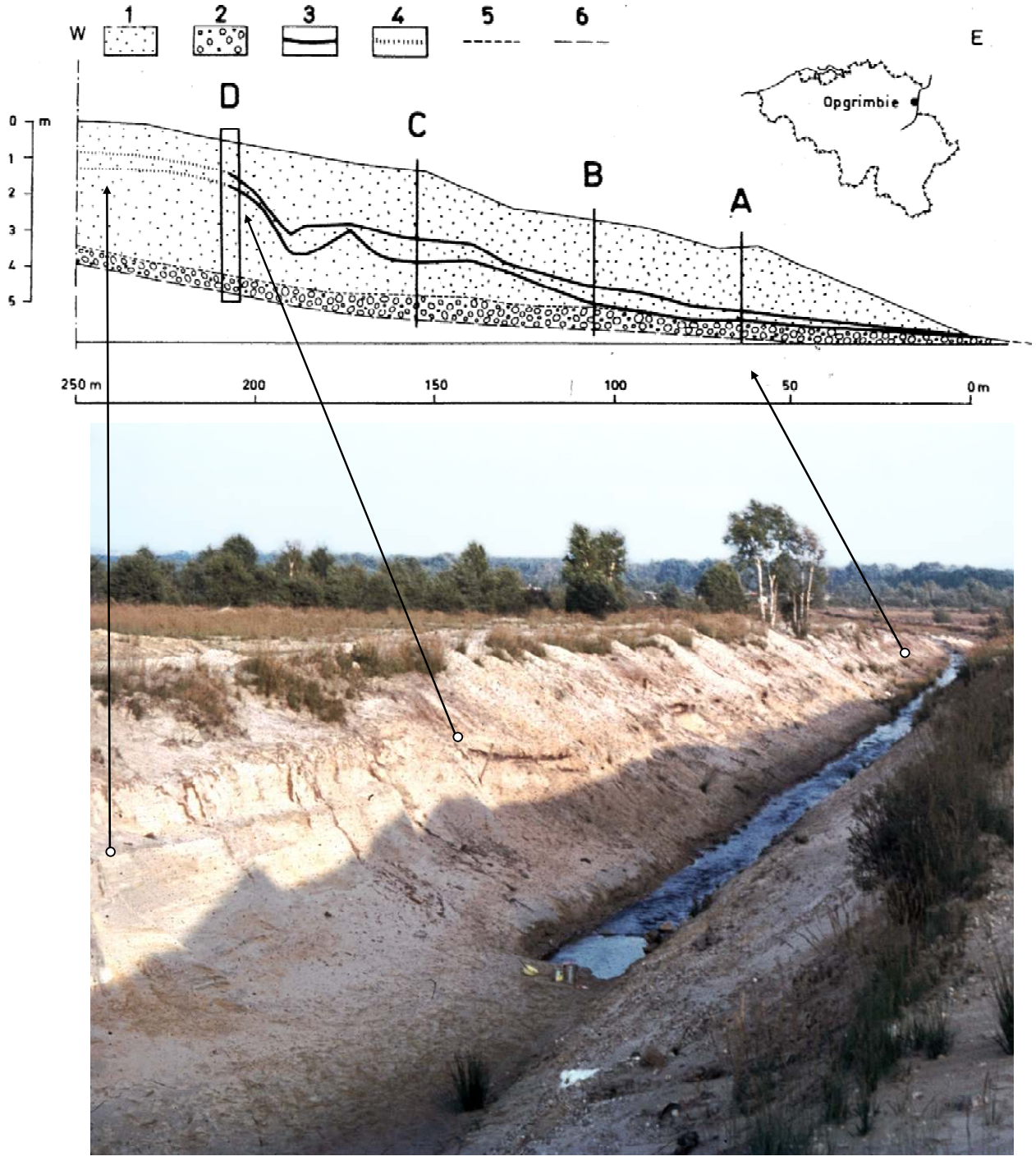

Fig. 57 - Opgrimbie: General section through the lee of the late glacial dune (Figure from Paulissen and Munaut, 1969). The section is photographed in 1968 (EP).

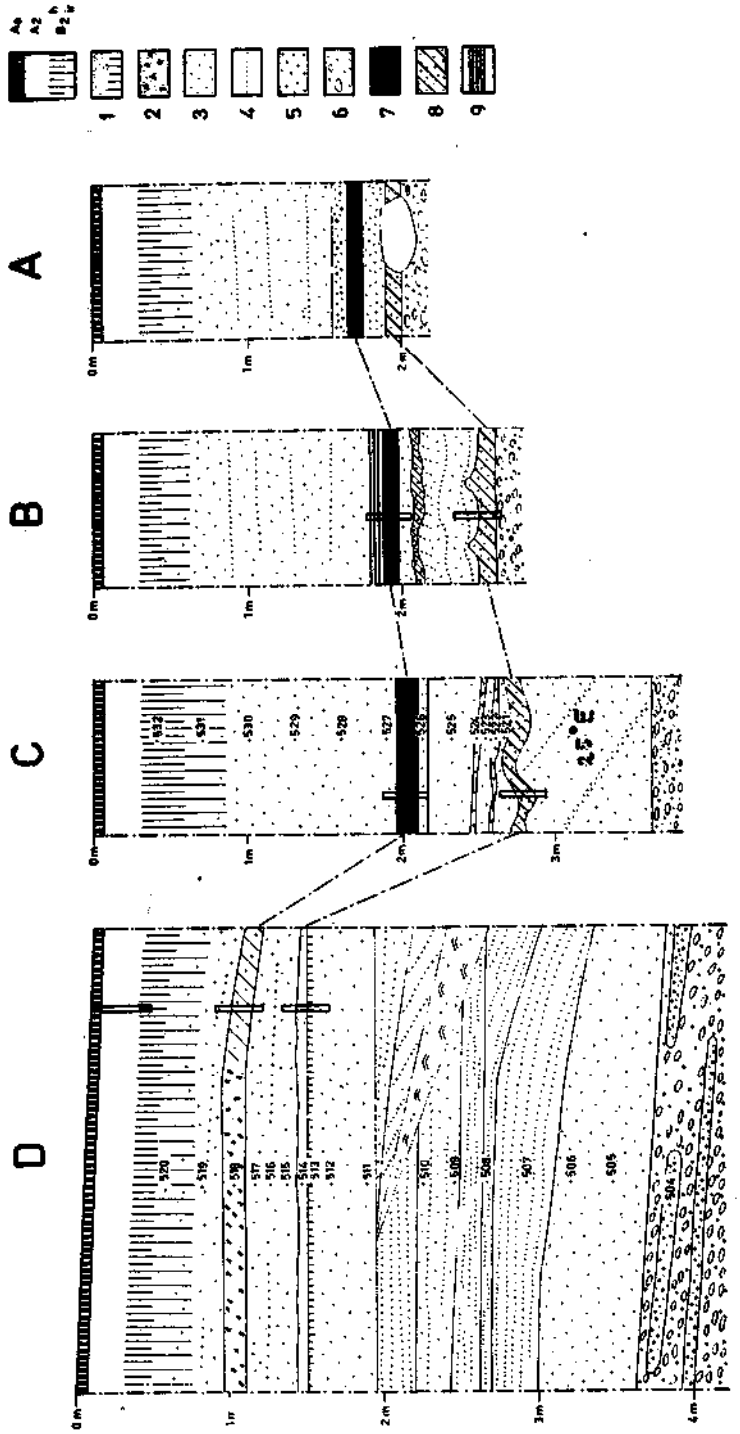

FIG. 2. Les profils détaillés.
1. horizon blanchâtre avec enrichissement à la base – 2. horizon blanchâtre avec des charbons de bois – 3. sable fin – 4. sable fin stratifié – 5. sable grossier – 6. gravier et sable grossier – 7. tourbe – 8. tourbe sableuse – 9. alternance de couches sableuses et tourbeuses.

Fig. 58 - Opgrimbie: Detailed sections A – D - for location see Fig. 57. (Figure from Paulissen et Munaut, 1969)

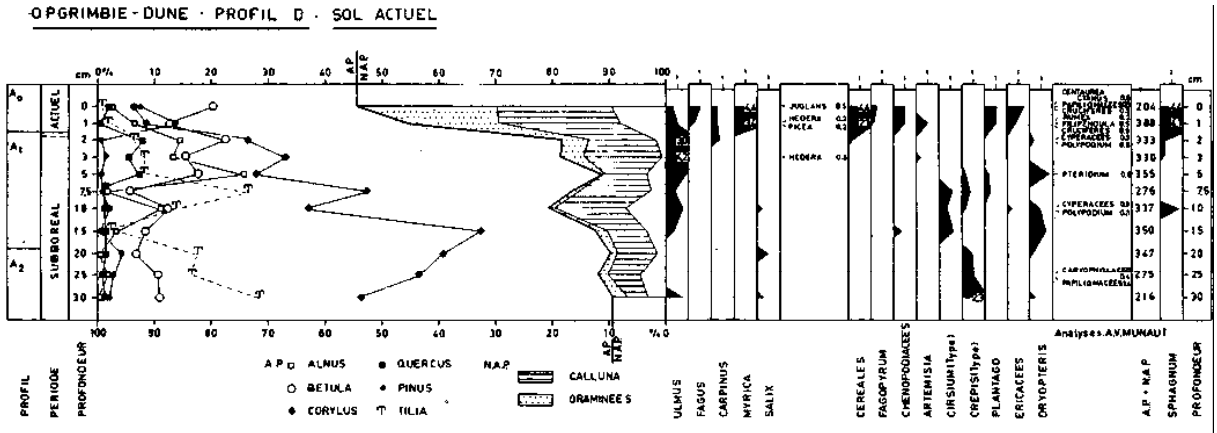

FIG. 9a. Diagramme pollinique du profil D : le sol actuel.

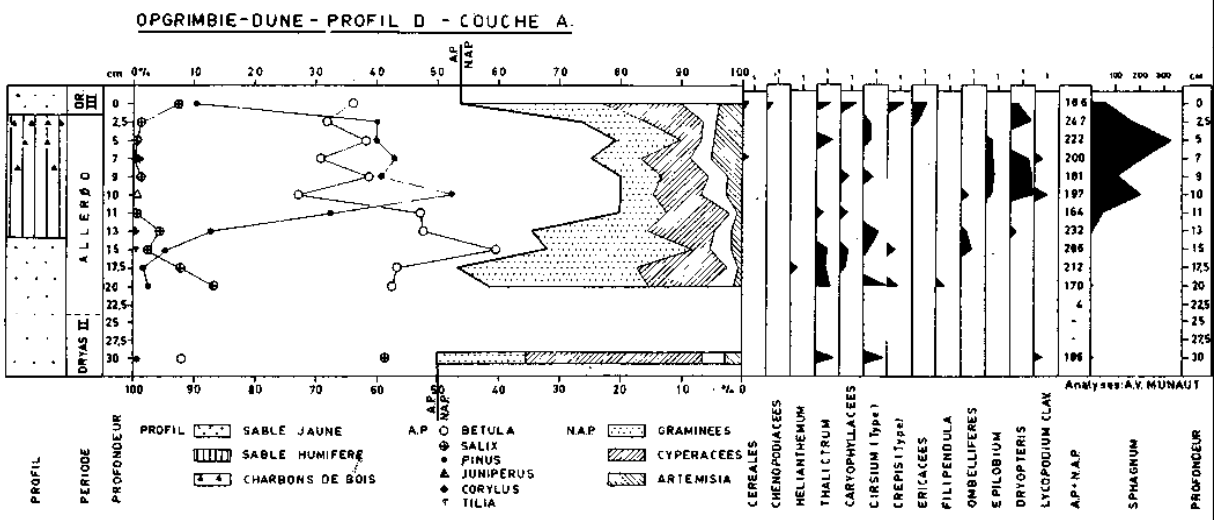

FIG. 9b. Diagramme pollinique du profil D : la couche A

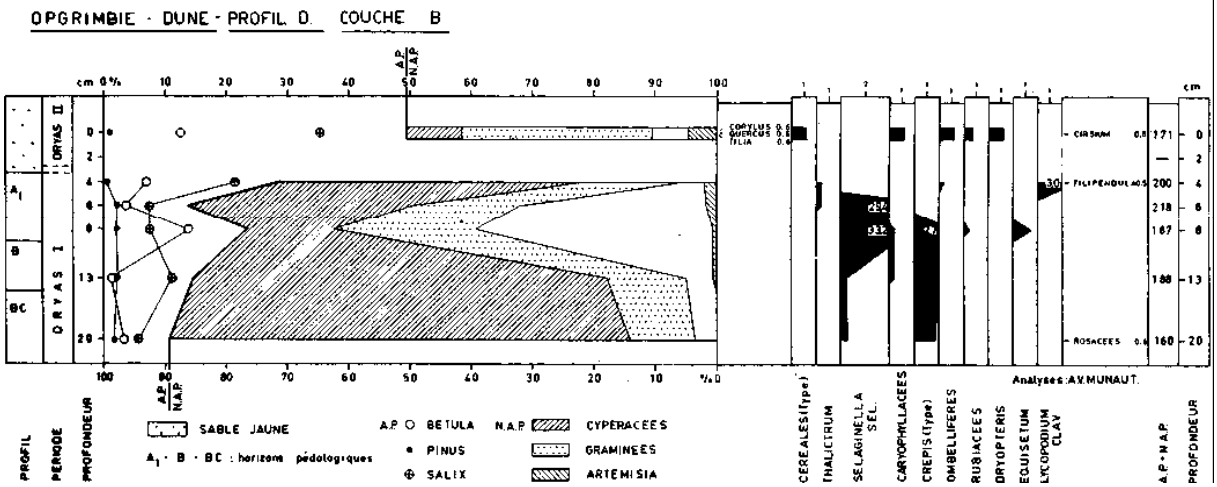

Fig. 59– Opgrimbie: Pollen profiles through the different sandy soil horizons in section D: the actual soil at the top – layer A (= Usselo Soil) in the middle – layer B (= Opgrimbie Soil) beneath. All analyses by the late André Mu-naut (figure from Paulissen et Munaut, 1969).

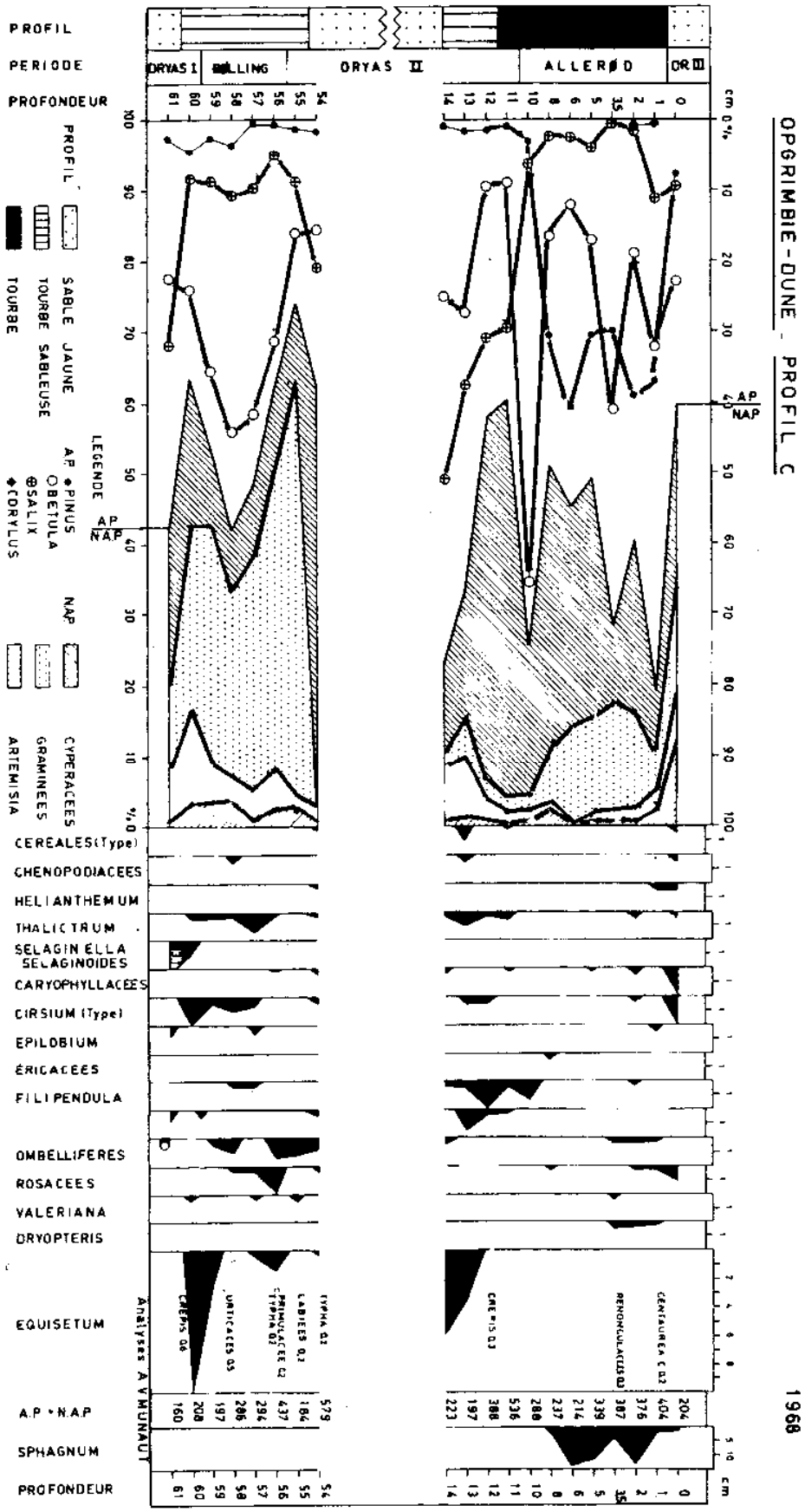

Fig. 60 – Opgrimbie: Pollen profile at section C through sandy peat layer B (= palynological stage Bölling – bulk sample 14C dated at 12,640 +/- 190 - Lv-456) and peat layer A (palynological stage Alleröd – bulk sample of peat 14C dated at 11,910 +/- 170 - Lv-456). The Alleröd period is interpreted to correspond locally with different types of deposits. All analyses by the late André Munaut (figure and 14C ages from Paulissen et Munaut, 1969)

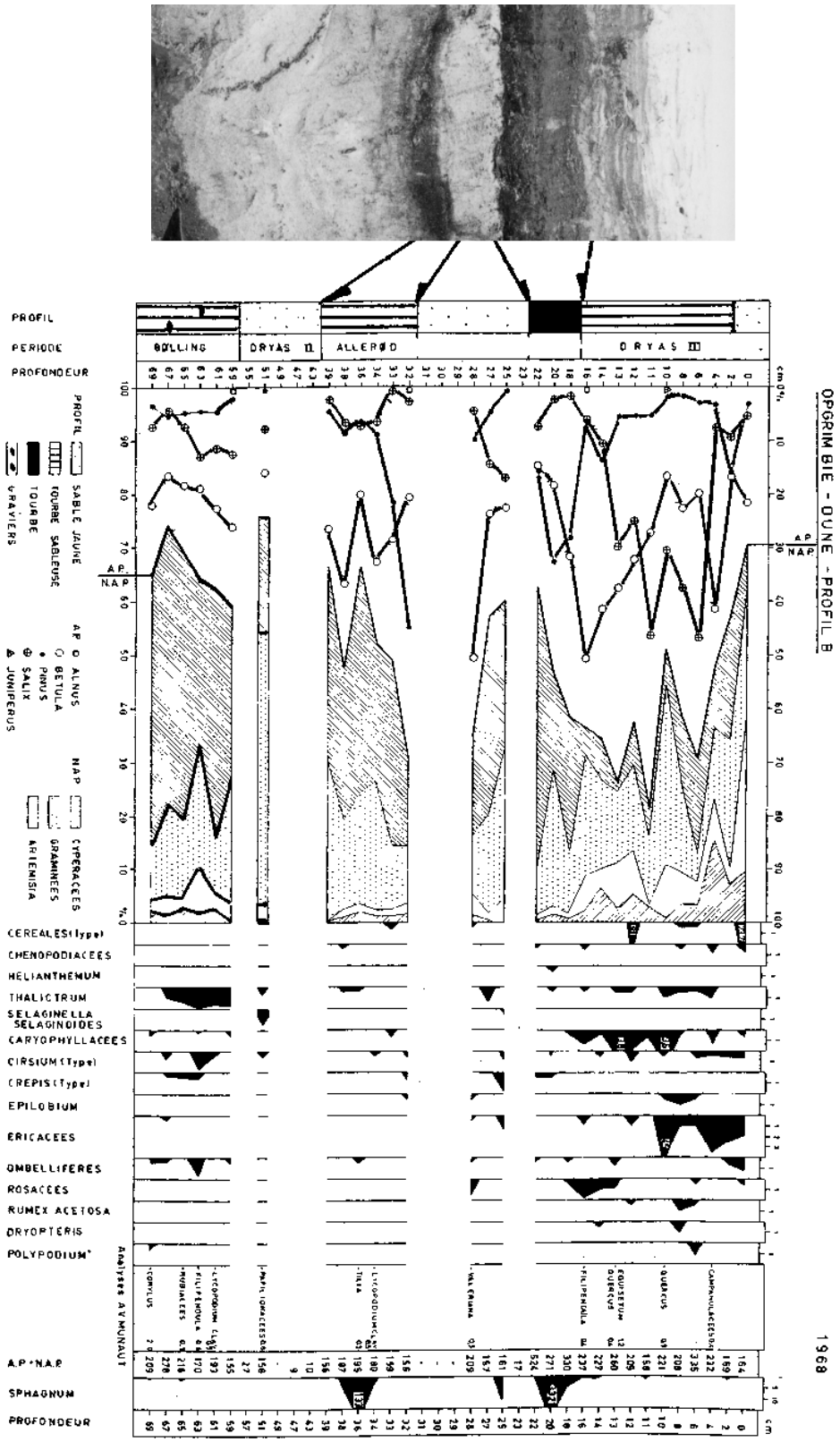

Fig. 61– Opgrimbie: Pollen profile at section B through sandy peat layer B and peat layer A (palynological stage. Alleröd – bulk sample of peat 14C dated at Lv-456). The Alleröd period is locally characterized by different types of deposits. All analyses by the late André Munaut (figure and 14C ages from Paulissen et Munaut, 1969)

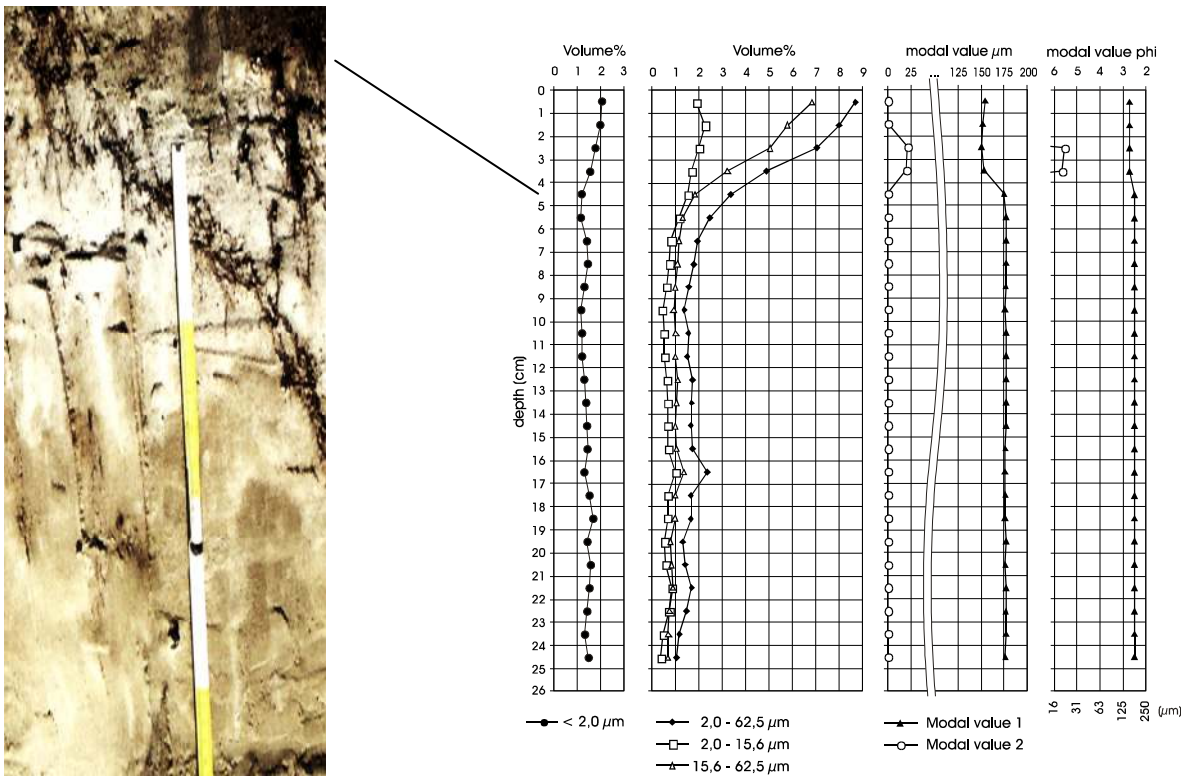

Opgrimbie - AMS Charcoal Ages from same bag from Usselo soil – All ages in cal yr BP (INTCAL04)

I. AMS ages on different charcoal pieces in same sample

	Probability 95.4%	Probability 68.2%	Intercept Age
Sample 1	13,190-12,930	13,140-12,960	13,080
Sample 2	13,870-13,590	13,810-13,660	13,740

II. AMS ages for individual charcoal pieces

	Probability 95.4%	Probability 68.2%	Intercept Age
Sample 3	13,420-13,200	13,360-13,240	13,290
Sample 4	13,750-13,150	13,550-13,250	13,370
Sample 5	13,850-13,250	13,690-13,390	13,490
Sample 6	13,780-13,300	13,680-13,410	13,550
Sample 7	14,000-13,350	13,840-13,530	13,720
Sample 8	13,940-13,650	13,850-13,710	13,780
Sample 9	14,120-13,710	14,000-13,790	13,850

Fig. 62: Opgrimbie – Section D – Usselo Soil: grain size and AMS dates on charcoal pieces within the Usselo Soil (all data unpublished)

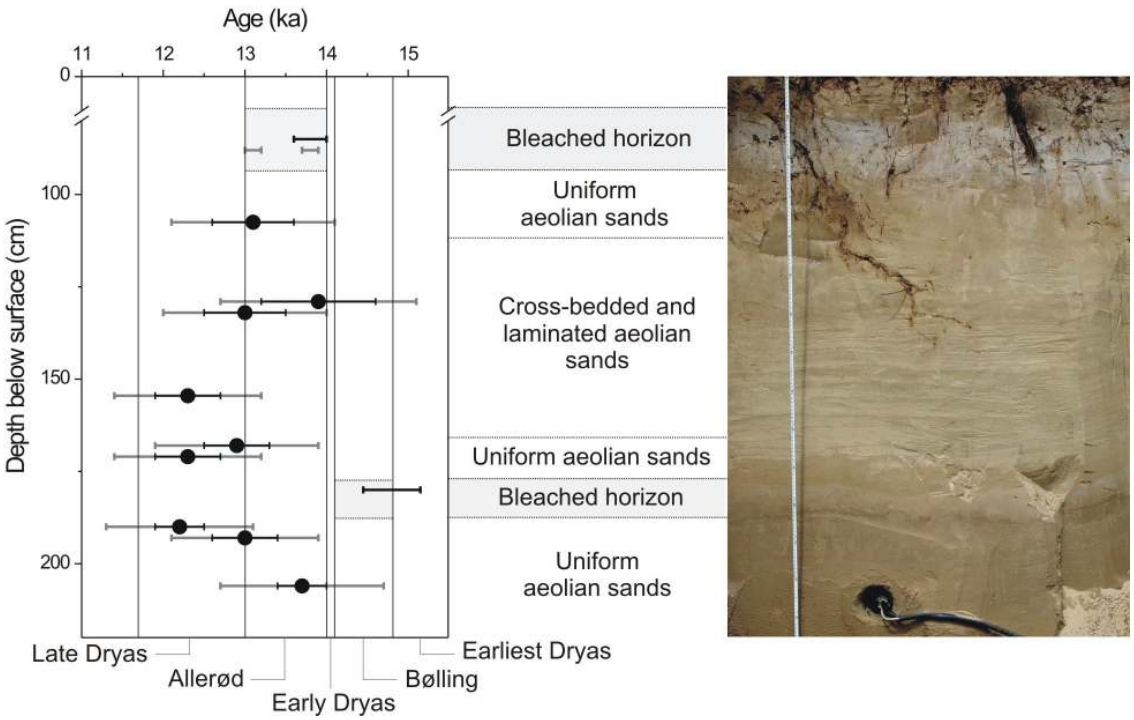

Fig. 63: Plot of the optical and radiocarbon ages against the depth below the surface. The optical ages are represented by black dots, while the associated random and total uncertainties are shown by black and dark grey error bars, respectively. The calibrated radiocarbon ages are represented as age ranges, the radiometric ages on the bulk samples in black and the AMS data on charcoal in dark grey. The vertical lines on the plot illustrate the 14C based age boundaries of the biostratigraphic units of the Late Glacial, as reviewed by Hoek (2001). The shaded areas show where the two bleached horizons are situated in the dune profile, as is also illustrated on the photograph. Figure taken from Derese et al. (2009).

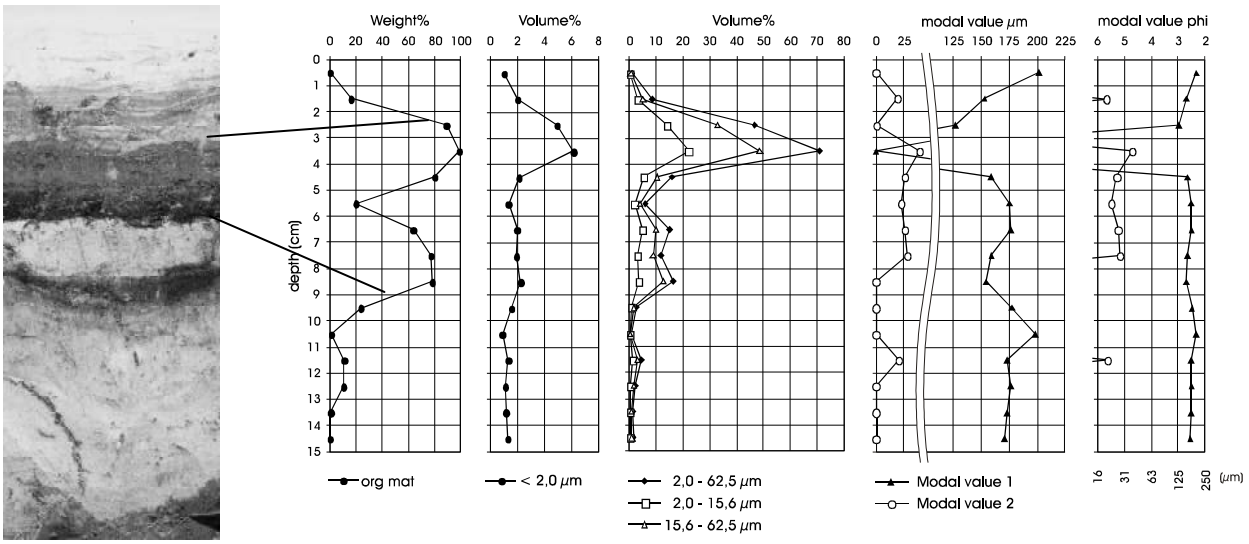

Peat of Alleröddage—detritic matter content and grainsize

Opgrimbie – Radiocarbon Ages from Peat Complex A

I. Age of bulk sample on peat (Lv-456 – Paulissen et Munaut, 1969)

Probability 95.4%: 14,110-13,640

II. AMS ages on uncharred shafts from the very bottom of the peat layer

	Probability 95.4%	Probability 68.2%	Intercept Age
Sample 1	13,670-12,480	13,740-13,420	13,610
Sample 2	13,640-13,460	13,720-13,400	13,570

III. AMS ages on uncharred remains from the lower sandy peat layer

	Probability 95.4%	Probability 68.2%	Intercept Age
Sample 3 (UP)	13,830-13,640	13,800-13,680	13,740
Sample 4 (UP)	13,760-13,470	13,740-13,570	13,670
Sample 5 (MP)	13,970-13,710	13,900-13,740	13,800
Sample 6 (MP)	13,900-13,660	13,840-13,710	13,770
Sample 7 (LP)	13,870-13,640	13,820-13,690	13,760
Sample 8 (LP)	13,310-13,130	13,280-13,180	13,240

Fig. 64: Opgrimbie – Section B – Alleröd Peat: organic matter content, grain size and AMS dates on uncharred short living plant remains (all data unpublished)

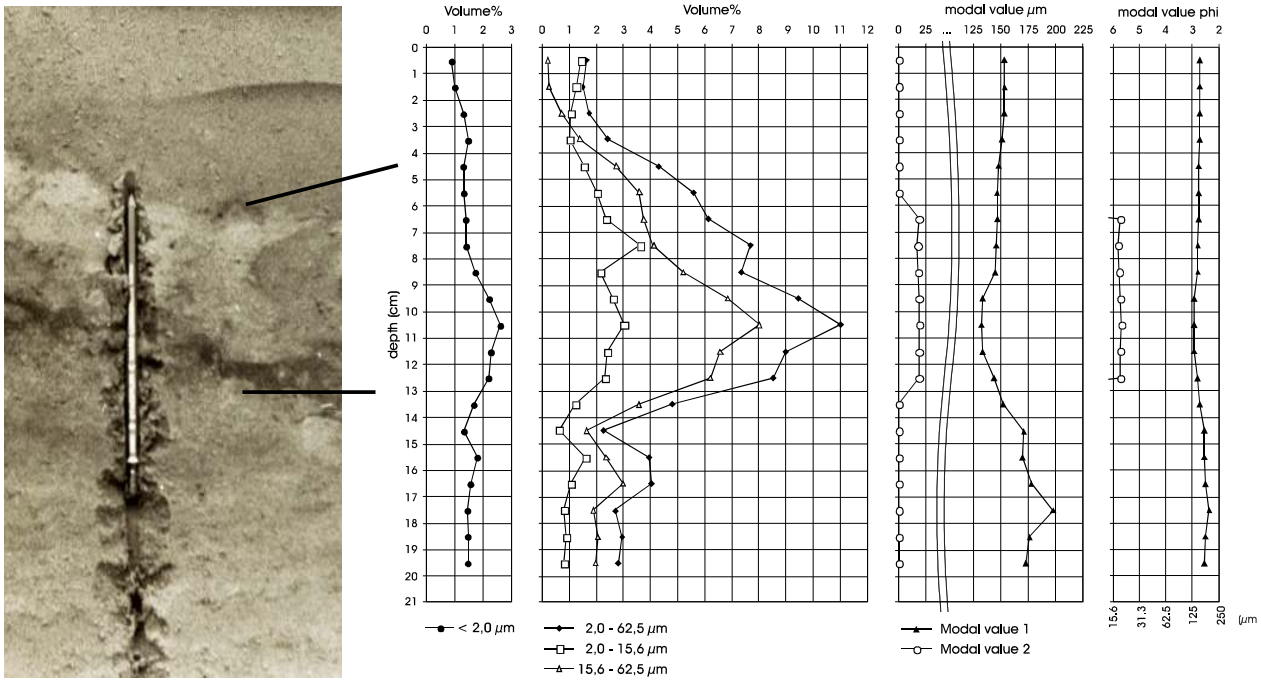

Opgrimbie – Radiocarbon Age from Peat Complex B, grading int the Opgrimbie soil

I. Age of bulk sample (Lv-457 – Paulissen et Munaut, 1969))

Probability 95.4%: 15,360-14,120

II. AMS dates are in progress

Fig. 65: Opgrimbie – Section D – Opgrimbie Soil: grain size (data unpublished)

References Opgrimbie

Derese, C., Vandenberghe, D., Paulissen, E., Van den haute, P., 2009, Revisiting a type locality for Late Glacial sand deposition in NW Europe: Optical dating of the dune complex at Opgrimbie (NE Belgium), *Geomorphology*, 109, 27-35. doi:10.1016/j.geomorph.2008.08.022.

Paulissen, E., Munaut, A.V., 1969, Un horizon blanchâtre d'age Bølling à Opgrimbie. *Acta Geographica Lovaniensia*, 7, 65–91.

References – selected for the Last Terminal

Firestone, R.B., West, A., Kenneth, J.P., Becker, L., Bunch, T.E., Revay, Z.S., Schultz, P.H., Belgya, T., Kennett, D.J., Erlandson, J.M., Dickenson, O.J., Goodyear, A.C., Harris, R.S., Howard, G.A., Kloosterman, J.B., Lechler, P., Mayewski, P.A., Montgomery, J., Poreda, R., Darrah, T., Que Hee, S.S., Smith, A.R., Stich, A.R., Topping, W., Wittke, J.H. & Wolbach, W.S., 2007, Evidence for an extraterrestrial impact 12.900 years ago that contributed to the megafaunal extinctions and the Younger Dryas cooling, *PNAS*, 104, 16016-16021.

Hoek, W.Z., 2001, Vegetation response to the ~ 14.7 and ~ 11.5 ka cal.BP climate transitions: is vegetation lagging climate? *Global and Planetary Change*, 30, 103–115.

Hoek, W.Z., 2008, The Last Glacial-Interglacial Transition, *Episodes*, 31, 226-229.

Lowe, J.J., Rasmussen, S.O., Björck, W.Z., Steffensen, J.P., Walker, M.J.C., Yu, Z.C., the INTIMATE group, 2008, Synchronisation of palaeoenvironmental events in the North Atlantic region during the Last termination: a revised protocol recommended by the INTIMATE group, *Quaternary Science Reviews*, 27, 6-17.

van der Hammen, T. & van Geel, B., 2008, Charcoal in soils of the Alleröd-Younger Dryas transition were the result of natural fires and not necessary the effect of an extra-terrestrial impact, *Netherlands Journal of Geosciences – Geologie en Mijnbouw*, 87, 359-361.